T CELLS

The gene regulatory basis of bystander activation in CD8$^+$ T cells

Neva B. Watson[1]†, Ravi K. Patel[2]†, Connor Kean[2]†, Janelle Veazey[1], Oyebola O. Oyesola[3], Nathan Laniewski[4], Jennifer K. Grenier[5], Jocelyn Wang[1], Cybelle Tabilas[1], Kristel J. Yee Mon[1], Adrian J. McNairn[5], Seth A. Peng[6], Samantha P. Wesnak[1], Kito Nzingha[7], Miles P. Davenport[8], Elia D. Tait Wojno[3], Kristin M. Scheible[9], Norah L. Smith[1], Andrew Grimson[2]*‡, Brian D. Rudd[1]*‡

CD8$^+$ T cells are classically recognized as adaptive lymphocytes based on their ability to recognize specific foreign antigens and mount memory responses. However, recent studies indicate that some antigen-inexperienced CD8$^+$ T cells can respond to innate cytokines alone in the absence of cognate T cell receptor stimulation, a phenomenon referred to as bystander activation. Here, we demonstrate that neonatal CD8$^+$ T cells undergo a robust and diverse program of bystander activation, which corresponds to enhanced innate-like protection against unrelated pathogens. Using a multi-omics approach, we found that the ability of neonatal CD8$^+$ T cells to respond to innate cytokines derives from their capacity to undergo rapid chromatin remodeling, resulting in the usage of a distinct set of enhancers and transcription factors typically found in innate-like T cells. We observed that the switch between innate and adaptive functions in the CD8$^+$ T cell compartment is mediated by changes in the abundance of distinct subsets of cells. The innate CD8$^+$ T cell subset that predominates in early life was also present in adult mice and humans. Our findings provide support for the layered immune hypothesis and indicate that the CD8$^+$ T cell compartment is more functionally diverse than previously thought.

INTRODUCTION

CD8$^+$ T cells play an essential role in protecting the host against intracellular pathogens. After infection, a small number of naïve CD8$^+$ T cells are activated via their T cell receptors (TCRs) by dendritic cells presenting microbial peptides in the context of major histocompatibility complex class I molecules (*1*). The activated CD8$^+$ T cells undergo clonal expansion and differentiate into various subsets of effector and memory cells (*2*, *3*). On the basis of their ability to respond to specific foreign antigens and form immunological memory, CD8$^+$ T cells are part of the adaptive immune system. However, a subset of naïve, antigen-inexperienced CD8$^+$ T cells can be activated during early stages of infection in an inflammation-dependent but TCR-independent bystander manner (*4*, *5*). Although bystander activation does not initiate robust proliferation, it results in the production of effector molecules, such as interferon (IFN-γ), which benefits the host by limiting pathogen growth (*6*, *7*). Thus, CD8$^+$ T cells are capable of protecting the host against infection via the canonical antigen-dependent (adaptive) response and also via the poorly understood antigen-independent (innate) response.

Previous studies have suggested that CD8$^+$ T cells produced in early life have more innate-like functions, whereas those generated in adulthood have more adaptive functions (*8*, *9*). For example, adult cells exhibit a diverse TCR repertoire and are efficient at generating memory cells after infection (*10*–*12*). Conversely, neonatal cells exhibit a narrowly restricted TCR repertoire composed of more germline-encoded TCRs and preferentially give rise to short-lived effector cells after infection. Another innate characteristic of neonatal CD8$^+$ T cells is that they express effector genes during thymic development and display a more effector-like chromatin landscape than their adult-derived counterparts even before stimulation (*13*, *14*). The distinct programming of neonatal and adult CD8$^+$ T cells relates to their derivation from different hematopoietic stem cell (HSC) progenitors (*13*, *14*). Neonatal CD8$^+$ T cells persist into adulthood and retain their innate-like properties, including an enhanced ability to produce IFN-γ in response to innate cytokines such as interleukin-12 (IL-12) and IL-18 (*13*). These findings place neonatal CD8$^+$ T cells in the same category as other innate-like lymphocytes [e.g., natural killer (NK) cells, innate lymphoid cells (ILCs), mucosal-associated invariant T cells (MAITs), NK T (NKT) cells, and γδ T cells], which exhibit an effector-like phenotype and can be activated by cytokines alone (*15*). However, unlike other innate-like T cells, the program of bystander activation in CD8$^+$ T cells remains largely undefined. For example, we do not know (i) what effector molecules [beyond IFN-γ and granzyme B (gzmB)] are produced by CD8$^+$ T cells after bystander activation, (ii) which gene regulatory mechanisms enable neonatal CD8$^+$ T cells to be highly responsive to innate cytokines, and (iii) whether the bystander program is conserved in mice and humans.

To address these questions, we used high-dimensional flow cytometry, RNA sequencing (RNA-seq), assay for transposase-accessible chromatin using sequencing (ATAC-seq), and single-cell profiling to identify the key epigenetic programs and transcription factors (TFs) that allow neonatal CD8$^+$ T cells to be more responsive to inflammation. We found that neonatal CD8$^+$ T cells are more responsive to innate cytokines not simply because they are poised to produce certain effector molecules but rather because they undergo extensive chromatin remodeling after stimulation, resulting in the availability of a

[1]Department of Microbiology and Immunology, Cornell University, Ithaca, NY 14853, USA. [2]Department of Molecular Biology and Genetics, Cornell University, Ithaca, NY 14853, USA. [3]Department of Immunology, University of Washington, Seattle, WA 98109, USA. [4]David H. Smith Center for Vaccine Biology and Immunology, Department of Microbiology and Immunology, University of Rochester Medical Center, Rochester, NY 14642, USA. [5]Genomics Innovation Hub and TREx Facility, Institute of Biotechnology, Cornell University, Ithaca, NY 14853, USA. [6]Department of Clinical Science, Cornell University, Ithaca, NY 14853, USA. [7]Institute for Immunology, University of Pennsylvania, Philadelphia, PA 19104, USA. [8]Kirby Institute for Infection and Immunity, UNSW Australia, Sydney, NSW 2052, Australia. [9]Department of Pediatrics, University of Rochester, Rochester, NY 14642, USA.
*Corresponding author. Email: bdr54@cornell.edu (B.D.R.); agrimson@cornell.edu (A.G.)
†These authors contributed equally to this work.
‡These authors contributed equally to this work.

multitude of activator protein 1 (AP-1) binding sites. As a consequence, neonatal CD8$^+$ T cells produce a broad spectrum of unexpected cytokines, which correspond to enhanced innate immune protection. In contrast, adult CD8$^+$ T cells are less capable of altering chromatin and instead express more Bach2, which blocks AP-1 binding. Collectively, our data suggest that the innate functions of neonatal CD8$^+$ T cells derive from their more permissive chromatin and altered usage of key TFs.

RESULTS

Neonatal CD8$^+$ T cells deploy a distinct program of bystander activation

The standard method for assessing innate functions of T lymphocytes is the bystander activation assay, where cells are cultured overnight in the presence of IL-2 alone (control group) or with IL-12 and IL-18 (stimulation group) and then evaluated for their ability to produce IFN-γ. However, there has not been a comprehensive and unbiased assessment of the effector molecules made by CD8$^+$ T cells after bystander stimulation. Moreover, we do not understand how the bystander program changes in CD8$^+$ T cells made at different stages of life. Thus, we performed the bystander activation assay on CD8$^+$ T cells from neonatal and adult TCR transgenic gBT-I mice (to ensure that all cells were antigen-inexperienced) and compared their gene expression profiles using RNA-seq (Fig. 1A and fig. S1A).

We first examined global differences in gene expression. Principal components analysis (PCA) revealed that neonatal cells have a transcriptome that is distinct from adults, both before and after undergoing bystander activation (Fig. 1B). Next, we used an "innateness" index of lymphocytes, which is based on the expression of innate genes (*16*) and found that neonatal cells were enriched for transcripts typically found in innate T cells (e.g., NKT, γδ, and MAIT cells), whereas adult cells were enriched for transcripts found in adaptive T cells (conventional CD4$^+$ T cells; Fig. 1C). These data suggest that neonatal CD8$^+$ T cells represent an intrinsically more innate-like lineage of cells than their adult counterparts.

It is possible that neonatal cells are not intrinsically more innate-like than adults but acquire this phenotype in the periphery. However, multiple pieces of data argue against this possibility. First, by comparing gene expression profiles of single-positive CD8$^+$ T cells in the thymus, we found that neonatal cells are more innate-like than adults before thymic export (fig. S1B) (*14*). Second, we found higher enrichment of innate genes in fetal-derived CD8$^+$ T cells when examining the transcriptomes of peripheral cells of the same age but derived from either fetal or adult progenitors (fig. S1C) (*14*). Third, we found that CD8$^+$ T cells from adult mice transgenic for Lin28b [the master regulator of fetal lymphopoiesis; (*17*)] also exhibit a higher innate index of gene expression (fig. S1D). These data support that innateness is intrinsically specified in neonatal CD8$^+$ T cells during early development.

To better understand how neonatal and adult CD8$^+$ T cells respond to innate cytokines, we performed gene set enrichment analysis (GSEA) and found that neonatal cells preferentially up-regulated genes associated with cytokine signaling and inflammatory responses, including IFN-γ and tumor necrosis factor–α signaling via nuclear factor κB (NF-κB; Fig. 1, D to F, and fig. S1E). We also examined the specific genes that were differentially expressed during bystander activation. Consistent with previous data (*14*, *18*), neonatal cells expressed higher levels of genes associated with innate lymphocytes (*Klrc1*, *Klrc2*, and *Nfil3*) and memory CD8$^+$ T cells (*Cd44*, *Tnfrsf9*, and *Tnfrsf8*) both before and after stimulation with innate cytokines (Fig. 1, G and H, and fig. S1, F and G). We also identified effector molecules that were up-regulated in neonatal cells after bystander stimulation (Fig. 1I and fig. S1H). As expected, neonatal cells expressed higher levels of *Ifng* and *GzmA* (gzmA), indicating that they respond more robustly than their adult counterparts. However, we also found that neonatal cells up-regulated a number of unexpected cytokines after stimulation, such as *Il13*, *Il22*, *Il10*, *Il17f*, and *Csf2* [granulocyte-macrophage colony-stimulating factor (GM-CSF)], many of which are not commonly associated with CD8$^+$ T cells. Thus, neonatal CD8$^+$ T cells undergo a distinct program of bystander activation.

Neonatal CD8$^+$ T cells provide innate protection against diverse pathogens

To validate our transcriptome profiling, we performed high-parameter flow cytometry and measured intracellular protein levels of cytokines secreted by neonatal and adult CD8$^+$ T cells after bystander activation (Fig. 2A). We found higher amounts of the unexpected cytokines (IL-13, IL-10, GM-CSF, and IL-17) in neonatal cells after stimulation (Fig. 2B and fig. S2, A to C). This distinct neonatal program of bystander activation was observed across a wide range of innate cytokine activation doses (fig. S3A) and was present in CD8$^+$ T cells from diverse tissues (fig. S3B). We also observed the same program in polyclonal CD8$^+$ T cells from neonatal C57BL/6 mice (fig. S3C) and monoclonal cells from OT-1 Rag$^{-/-}$ mice (fig. S3D), indicating that the neonatal bystander program is found in diverse strains and represents a common feature of CD8$^+$ T cells made in early life.

We also investigated the types of stimuli required for the bystander response. Although IL-12 and IL-18 synergized to induce robust production of classical effector molecules (e.g., IFN-γ and gzmB), stimulation with either cytokine was sufficient to promote secretion of unexpected cytokines (IL-13 and IL-17f) from neonatal but not adult CD8$^+$ T cells (fig. S3E). The ability of neonatal cells to respond did not appear to correspond to changes in the expression of IL-12 or IL-18 receptors because these receptors were expressed at comparable levels in cells from neonatal and adult mice (fig. S3F). To determine whether the distinct cytokine profiles observed in neonatal cells were restricted to innate stimuli, we stimulated adult and neonatal cells via the TCR with anti-CD3 and anti-CD28 antibodies. PCA of flow cytometry data showed that neonatal samples exhibit a cytokine profile distinct from their adult counterparts when stimulated with innate cytokines but not when activated via the TCR (fig. S4A). Thus, neonatal cells do not produce unexpected cytokines in response to all forms of activation but are particularly responsive to innate cytokines.

The robust program of bystander activation in neonatal CD8$^+$ T cells prompted us to ask whether they could provide enhanced immune protection in a TCR-independent manner. Thus, we performed adoptive transfers of monoclonal TCR-transgenic populations of neonatal or adult donor cells into T cell-deficient recipients and infected them with a strain of *Listeria monocytogenes* lacking the cognate ligand for the TCR [wild type (WT)–LM] (Fig. 2C). Despite the absence of TCR signaling, recipients receiving neonatal donor CD8$^+$ T cells had reduced pathogen burdens compared with animals receiving adult cells (Fig. 2D). The enhanced ability of neonatal CD8$^+$ T cells to protect the host against unrelated pathogens could not be explained by an increase in the number of donor cells during

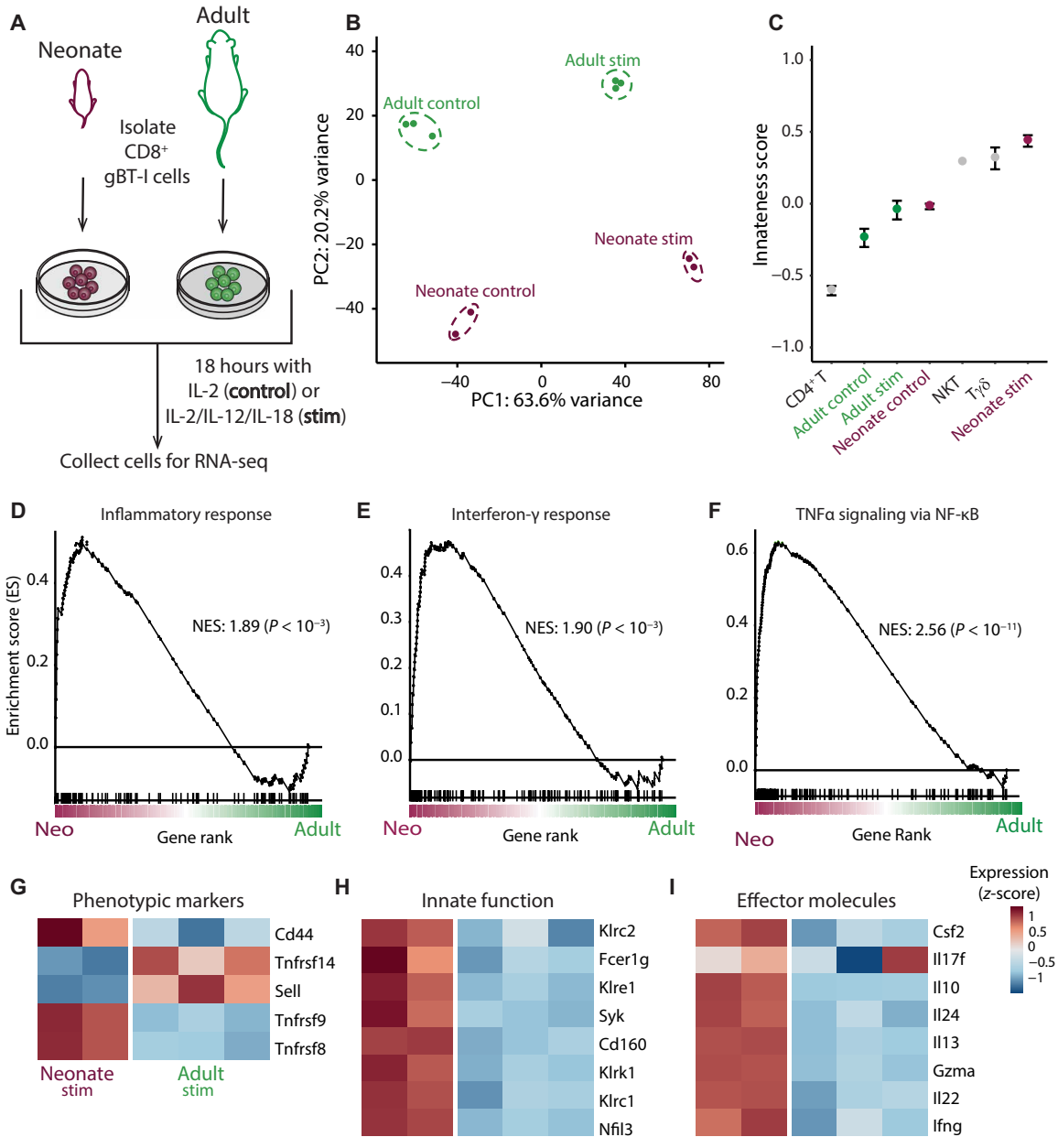

Fig. 1. Neonatal CD8$^+$ T cells have a distinct program of bystander activation. (**A**) Adult or neonate CD8$^+$ T cells were stimulated overnight with IL-2 ± IL-12/18 and gene expression determined by RNA-seq. (**B**) PCA of samples described in (A); $n = 2$ or 3 mice. (**C**) Median innateness score (negative = high adaptiveness, positive = high innateness), including CD4$^+$ T, NKT, and γδ T cells from ImmGen dataset (GSE109125). Error bars represent SD across replicates. (**D** to **F**) GSEA running enrichment score plots for three selected Hallmark pathways significantly up-regulated in neonatal cells upon IL-12/18 stimulation compared with that in adults [gene rank expressed as mean $\log_2$(stim/control)]. TNFα, tumor necrosis factor–α; NES, normalized enrichment score. CFU, colony-forming units. (**G** to **I**) Heatmap visualization of row-scaled gene expression of noteworthy phenotypic (G), innate (H), and effector (I) markers in adult and neonatal cells under IL-2 + IL-12/18 treatment. For each heatmap, the three left and two right columns correspond to adult and neonate replicates, respectively.

infection (fig. S4B), and neonatal cells were also capable of limiting bacterial growth in young B6 recipients (fig. S4C).

A potential explanation for the ability of neonatal CD8$^+$ T cells to provide enhanced innate immune protection against intracellular bacteria is through an IFN-γ–dependent mechanism (*19*). However, when we tested neonatal donor cells from gBT-I IFN-γ knockout mice, we observed no impairment in their ability to provide bystander protection (fig. S4D). Because neonatal cells produce a variety of other cytokines after bystander activation, we next investigated whether they could provide innate-like protection against different pathogens (e.g., helminths and viruses), which rely on more diverse cytokines, including IFN-γ, IL-13, and GM-CSF, for protection (*19*–*21*). Mice receiving neonatal cells displayed reduced *Nippostrongylus brasiliensis* worm burdens (Fig. 2E) and decreased influenza viral copies concomitant with less weight loss compared with those receiving adult donor cells (Fig. 2F). These findings suggest that a major function

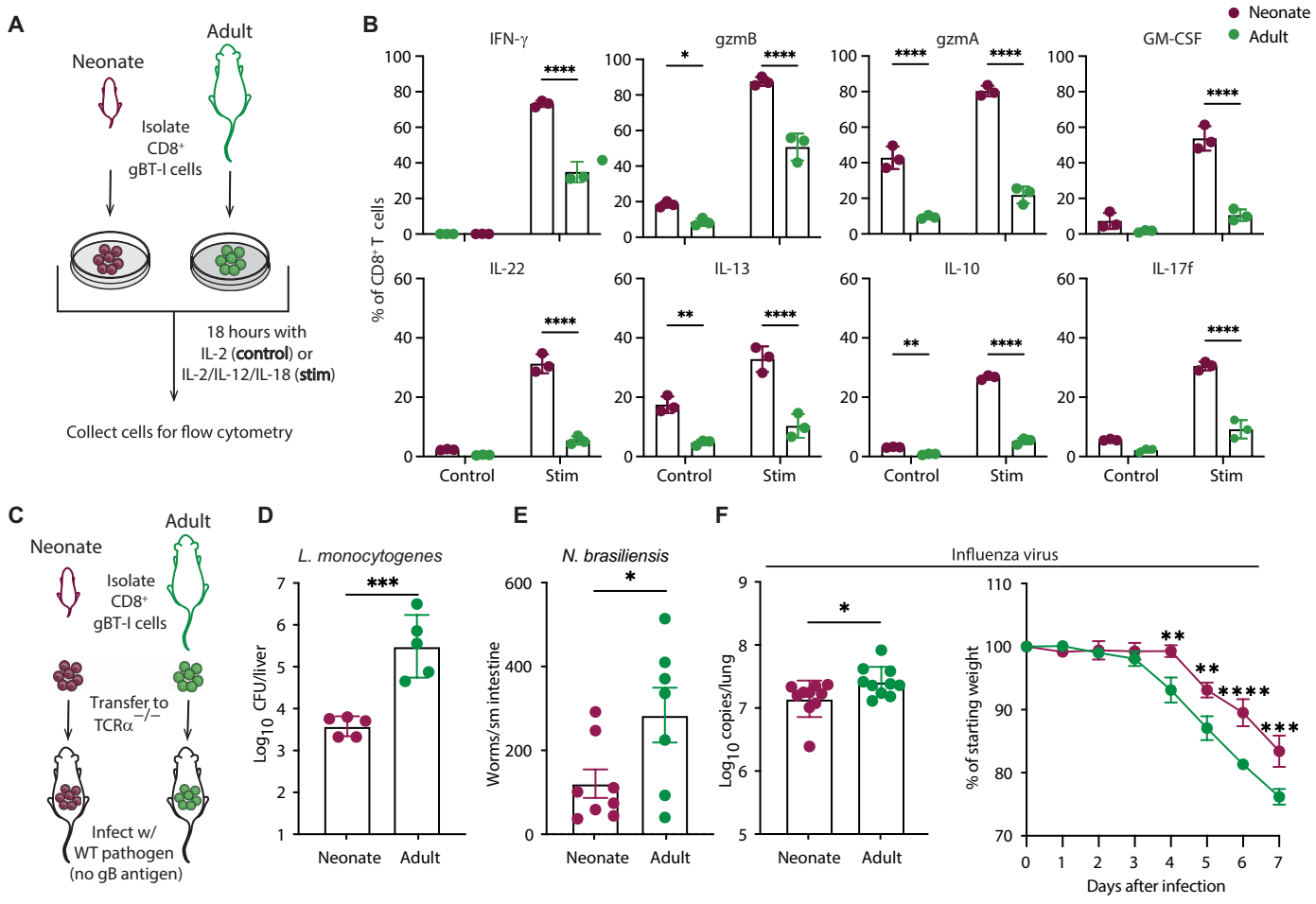

Fig. 2. Neonatal CD8$^+$ T cells provide enhanced innate protection against unrelated pathogens. (**A**) Neonate or adult CD8$^+$ T cells were stimulated overnight with IL-2 ± IL-12/18, and cytokine expression was analyzed by flow cytometry. (**B**) Percentages of live CD8$^+$ T cells expressing different cytokines; representative of four independent experiments. Two-way ANOVAs were performed with Šidák's multiple comparison test. (**C**) TCRα$^{-/-}$ recipients received gBT-I CD8$^+$ T cells and were inoculated with irrelevant pathogens (i.e., non-gB expressing) the following day. (**D** to **F**) Pathogen loads shown for indicated tissues and time points after infection with *L. monocytogenes* (3 dpi, D), *N. brasiliensis* (10 dpi, E), and influenza virus pathogen load and weight loss (7 dpi, F). To determine statistical significance, unpaired *t* tests and two-way repeated-measures ANOVA followed by Šidák's multiple comparison test between neonate and adult at each time point were performed for pathogen burden and weigh loss measurements, respectively. Two pooled experiments shown for path burden experiments and one representative experiment shown for influenza virus (performed in duplicate); $n = 4$ to 9. For statistical comparisons, $^*P < 0.05$, $^{**}P < 0.01$, $^{***}P < 0.001$, and $^{****}P < 0.0001$.

of neonatal CD8$^+$ T cells is to provide an innate-like response during primary infection, whereas adult CD8$^+$ T cells use classical adaptive responses and offer protection against secondary infections.

Neonatal CD8$^+$ T cells are composed of multiple innate subsets

Previous work has shown that neonates have a large subset of antigen-inexperienced CD8$^+$ T cells (denoted virtual memory), distinguished by their ability to respond to innate cytokines (*14*, *22*, *23*). Thus, neonatal CD8$^+$ T cells may be more responsive to innate cytokines than adult cells because they contain a larger fraction of virtual memory cells. To examine this possibility, we isolated virtual memory (CD44^{hi} CD122^{hi}) cells from neonatal and adult gBT-I mice and compared the ability of phenotype-matched subsets from different-aged mice to undergo bystander activation. In the presence of IL-2 alone, virtual memory cells from neonatal and adult mice expressed comparably low amounts of effector molecules (fig. S5A). However, with the addition of IL-12 and IL-18, we found that neonatal virtual memory cells produced substantially more GzmA, GzmB, and IFN-γ than adult virtual memory cells (fig. S5A). Thus, neonatal CD8$^+$ T cells undergo more bystander activation than adult cells not because they contain more virtual memory cells but rather because these cells are inherently more sensitive to innate cytokine stimulation.

To comprehensively examine the diversity of neonatal subsets capable of responding to bystander activation, we generated single-cell RNA-seq (scRNA-seq) datasets from the same four populations profiled by bulk RNA-seq (Fig. 3A). First, we confirmed that the age-related differences identified by RNA-seq were recapitulated by scRNA-seq by showing that the expression of cytokines specifically expressed in neonates were expressed in a higher proportion of neonatal cells and at higher levels compared with adult counterparts (fig. S5B). To define functionally diverse subsets, we visualized the single-cell data in two-dimensional space using uniform manifold approximation and projection (UMAP) and used Seurat to cluster the individual samples before (fig. S5C) and after bystander activation (Fig. 3B) (*24*), which uncovered distinct subsets of neonatal and adult

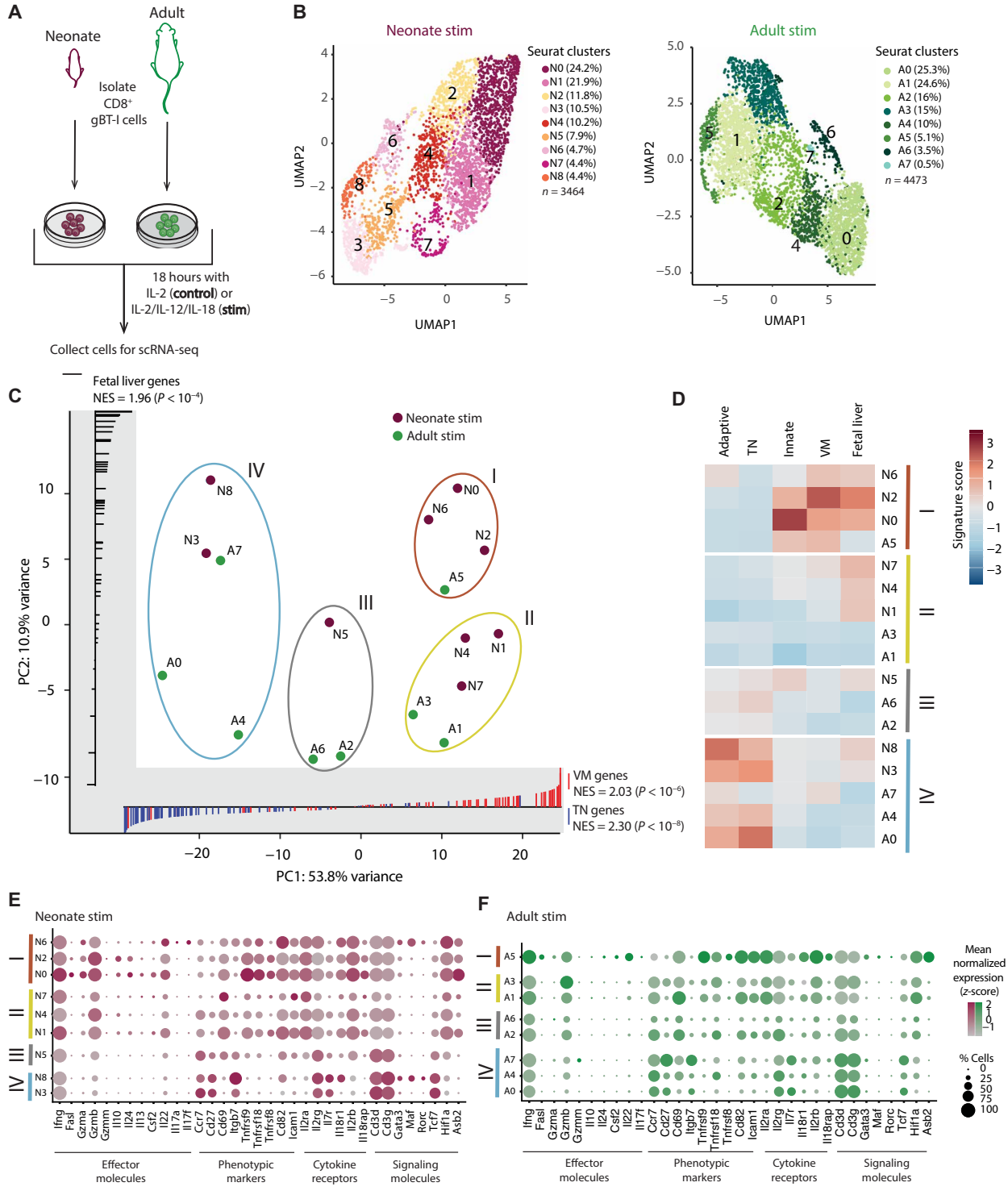

Fig. 3. CD8$^+$ T cells are composed of multiple subsets with distinct innate properties. (**A**) Neonate (cell $n = 3464$) and adult (cell $n = 4473$) CD8$^+$ T cells were stimulated overnight with IL-2 ± IL-12/18, and live CD8$^+$ T cells were sorted for scRNA-seq ($n = 1$; for neonates, three or four mice were pooled). (**B**) UMAP visualization of scRNA-seq data from neonate and adult samples. Subset identities overlaid and differentially colored with the subset size conveyed as a percentage of the total population in parentheses. (**C**) PCA plot of pseudo-bulk gene expression profiles of subsets from (B); subsets with similar gene expression profiles were assigned a group number (I to IV). GSEA gene rank plots (inset) depict the enrichment of virtual memory (red) and true naïve (blue) gene sets among genes with positive and negative PC1 loadings, respectively (*x* axis) and of the fetal-liver (black) gene set in genes with positive PC2 loadings (*y* axis). The NES and adjusted *P* values are indicated. (**D**) Column-scaled gene set signature scores derived from pseudo-bulk expression profiles of subsets. Subsets are ordered by group corresponding to (C). (**E**) Bubble plots of selected effector molecules, phenotypic markers, cytokine receptors, and signaling molecules by subset within neonatal (left) or adult (right) cells. Dot shading indicates the mean normalized expression (*z*-score), and dot size represents percent of cells expressing the genes. Subsets are ordered by group corresponding to (C).

cells. Projection of all subsets from either the control or stimulated group onto a single PCA plot uncovered the differential capacity of both adult and neonatal subsets to mount a bystander transcriptional response (fig. S5, D and E).

To focus on how neonatal and adult CD8$^+$ T cells differentially respond to bystander stimulation, we examined the transcriptomes of the bystander stimulated subsets and identified four groups (I to IV) (Fig. 3C). Each group had a distinct combination of gene signatures (true naive, virtual memory, innate, adaptive, and fetal liver) (Fig. 3D and fig. S5F). We asked whether we could use these groups to determine whether neonatal virtual memory cells are particularly sensitive to innate cytokine stimulation because they are derived from fetal progenitors (*13*, *14*), which tend to give rise to lymphocytes that display innate-like functions (*17*, *25*). To explore this possibility, we classified the four groups into virtual memory versus true naïve T cells and fetal-derived versus adult-derived T cells, evaluating the enrichment of virtual memory (*13*) and fetal progenitor (*26*, *27*) gene sets. Principal component 1 (PC1) loadings distinguish virtual memory cells from true naïve cells, whereas PC2 loadings separate fetal-derived from adult-derived subsets (Fig. 3C). Thus, subsets of cells in the top right of the PCA plot (group I of Fig. 3C) correspond to virtual memory cells derived from fetal HSCs. This group was composed of three neonatal subsets (N0, N2, and N6; 40% of the neonatal cells) and also a single adult subset (A5; 5% of the adult cells). A5 likely represents the subpopulation of neonatal cells that persist into adulthood and retain their innate-like functions (*13*, *28*). The subsets of cells in the lower right of the PCA plot (group II) correspond to virtual memory cells derived from adult HSCs. This group contained two adult subsets (A1 and A3; 40%) and three neonatal subsets (N1, N4, and N7; 36%), consistent with previous work showing some HSCs have adult transcriptional identities at birth (*29*). The remaining groups (III and IV) were composed of neonatal and adult subsets that have a more naïve phenotype.

The group I subsets (fetal-derived, virtual memory cells) could be distinguished from group II subsets (adult-derived, virtual memory cells) in a number of ways. First, group I subsets exhibited a higher innateness score, suggesting a relationship between CD8$^+$ T cells made in early life and innate immune activation (Fig. 3D). Second, group I subsets expressed lower levels of genes characteristic of naïve T cells (*Cd3d*, *Cd3g*, *Sell*, *Il7r*, *Ccr7*, and *Tcf7*), which may relate to their ability to be activated by cytokines alone (Fig. 3, E and F). Third, group I corresponded to cells expressing distinct combinations of cytokines *(l13*, *Il22*, *Il10*, *Il17f*, and *Csf2*) not conventionally associated with CD8$^+$ T cells (Fig. 3, E and F). The neonatal cells (N6) that preferentially expressed IL-17 and IL-22 expressed factors (*Maf*, *Rorc*, and *Hif1a*) characteristic of T helper 17 (T_H17) cells, NKT17 cells, and γδ17 cells (*30*, *31*). Similarly, the neonatal cells (N0 and N2) that expressed *Il13*, *Il10*, and *Csf2* also expressed *Asb2*, which is normally found in T_H2 cells, ILC2s, or macrophages (*32*). These findings indicate that there is higher diversity in the neonatal virtual memory pool compared with that in the adult virtual memory pool and that unexpected innate cytokines are produced by the most fetal-like subsets of cells, including a subset found in adults.

Neonatal CD8$^+$ T cells undergo extensive chromatin remodeling after stimulation

We next sought to determine why neonatal CD8$^+$ T cells can respond so rapidly to innate cytokines. On the basis of our previous work (*13*), we hypothesized that neonatal cells are capable of rapidly producing cytokines because the corresponding loci are more accessible before stimulation [akin to ILCs; (*33*)]. However, we also considered whether neonatal cells are more responsive because they can more rapidly remodel their chromatin after stimulation, similar to macrophages (*34*) or NK cells (*35*). To distinguish between the "poised" and "remodeling" models, we used the ATAC-seq and compared the chromatin landscape of neonatal and adult cells before and after undergoing bystander activation (Fig. 4A).

The PCA of chromatin accessibility recapitulated the patterns observed in transcriptional profiling, with the first PC distinguishing the activation status and the second separating the developmental origins of the samples (Fig. 4B). To establish a link between age-related gene expression and accessibility, we performed differential accessibility testing on the peaks at loci of genes encoding cytokines preferentially expressed in neonatal cells after bystander activation. This testing revealed differences both before and after activation; however, differences were more pronounced after activation (Fig. 4C). Thus, neonatal cells undergo a diverse and robust program of bystander activation both because they are poised to express cytokines and also because they undergo more extensive chromatin remodeling upon stimulation, thereby enabling cytokine expression.

Given the dynamic changes in chromatin accessibility by neonatal cells, we systematically compared changes in candidate enhancer (ATAC-seq peaks) accessibility in both groups of CD8$^+$ T cells before and after stimulation. We classified the up-regulated enhancers on the basis of whether they were also accessible in the resting state (poised enhancers) or only after stimulation (de novo enhancers) (Fig. 4D). In CD8$^+$ T cells produced in early life, we found a large number of poised enhancers that were accessible under basal conditions and significantly more accessible upon stimulation (Fig. 4, D and E). We also found that neonatal cells had a set of de novo enhancers, unveiled only after innate cytokine exposure (Fig. 4E). Neonatal cells had far more poised and de novo enhancers than adult cells, and these enhancers displayed significant enrichment of basic leucine zipper (bZip) TF (e.g., AP-1) binding motifs (fig. S6, A and B).

To understand the role of these poised and de novo enhancers, we asked whether the genes associated with neonatal-specific enhancers overlapped with genes whose expression characterized the neonatal bystander transcriptional response (Fig. 4F). The 438 genes associated with the presence of both de novo and poised neonatal-specific putative enhancers were associated with the neonatal bystander transcriptional response, whereas genes associated with either type of enhancer alone were not (Fig. 4G). Moreover, the genes associated with both de novo and poised enhancers were preferentially up-regulated in innate lymphocytes (NKT cells, γδT cells, and NK cells) (Fig. 4H) and enriched in pathways related to innate defense, cytokine signaling, and T cell activation (Fig. 4I). These data suggest that the combination of de novo and poised enhancers present in CD8$^+$ T cells produced in early life facilitate their rapid innate functions and identify a set of genes that contribute to innate functions in CD8$^+$ T cells. Thus, the neonatal bystander response shares attributes of different innate cells, incorporating both poised enhancers primed to respond (akin to ILCs) and those that become accessible only after stimulation (akin to macrophages and NK cells).

We also asked what developmental-related factor(s) might enable neonatal CD8$^+$ T cells to undergo rapid chromatin remodeling. Previously, we showed that ectopic expression of $Lin28b^{17}$ was sufficient to induce adult CD8$^+$ T cells to mimic neonatal cells (*10*, *14*). However, these studies were performed in the context of TCR stimulation. To

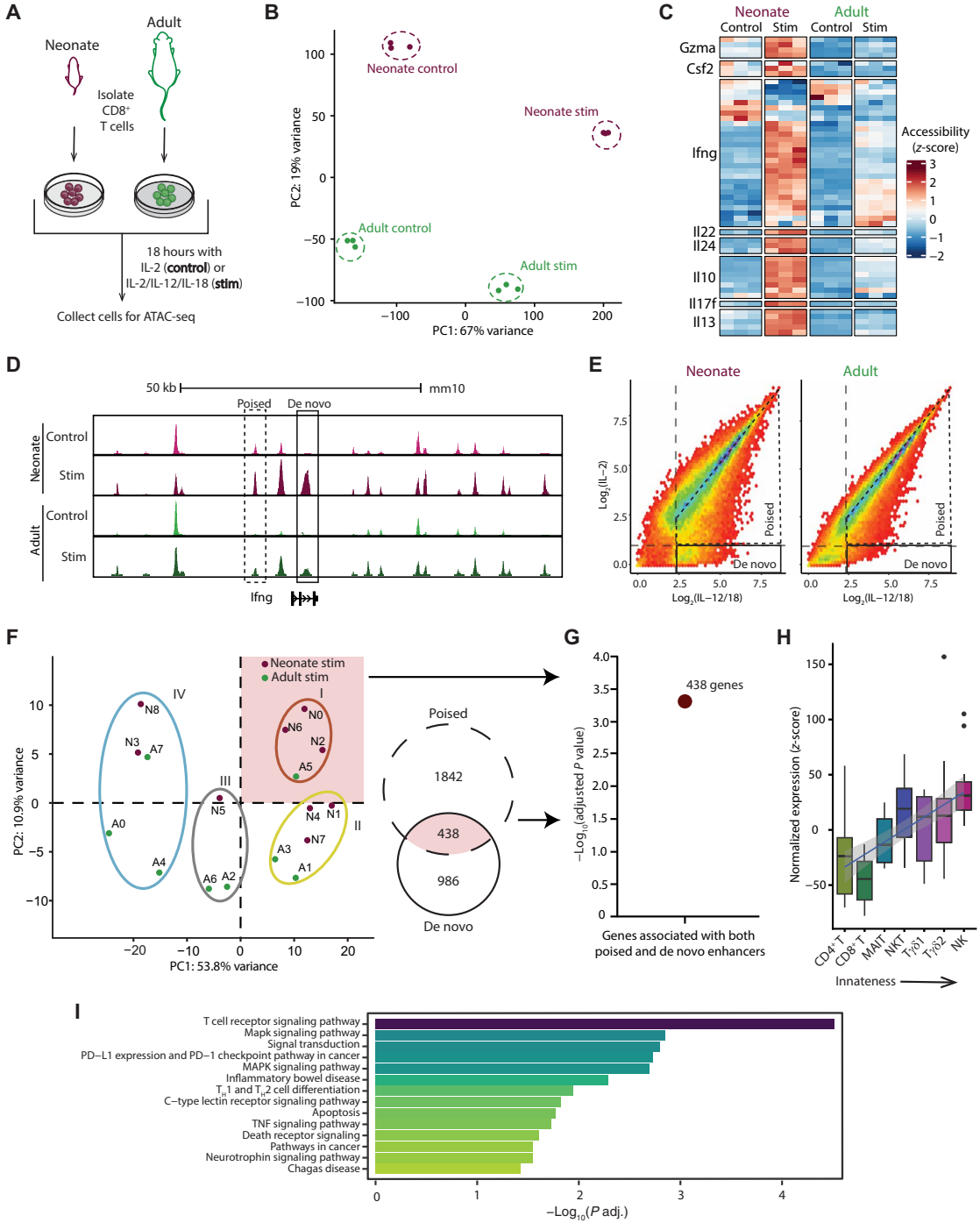

Fig. 4. Neonatal CD8$^+$ T cells undergo chromatin remodeling in response to inflammatory signals. (**A**) Neonate or adult CD8$^+$ T cells were stimulated overnight with IL-2 ± IL-12/18 and analyzed by ATAC-seq. (**B**) PCA of ATAC-seq profiles ($n = 3$ mice per group). (**C**) Heatmap visualization of ATAC-seq peak intensities for indicated genes. Intensities determined by row-wise *z*-scores of reads per million. All displayed peaks are differentially expressed between adults and neonates either in control samples or after bystander stimulation. (**D**) Genome browser view showing chromatin accessibility for de novo (solid box) and poised (dashed box) enhancers at the *Ifng* locus. (**E**) Scatter plot of chromatin accessibility at ATAC-seq peaks for adult (left) and neonate (right) CD8$^+$ T cells, colored by two-dimensional density. Dashed horizontal and vertical lines represent the accessibility cutoffs chosen to identify de novo (solid box) and poised (dashed trapezoid) enhancers (see Materials and Methods). (**F** and **G**) Genes with positive PC1 and PC2 loadings (1242 genes) from scRNA-seq PCA were extracted to compare with genes putatively regulated by poised enhancers only (1842 genes), both poised and de novo enhancers (438 genes, highlighted) and de novo enhancers only (986 genes). Significance of enrichment reported as the $-\log_{10}$(adjusted *P* value). (**H**) Distributions of aggregated levels (see Materials and Methods) of genes putatively regulated by both de novo and poised enhancers across replicates in various human immune cells (obtained from GSE124731). Samples ordered (*x* axis) by increasing innateness potential. The aggregation was performed by addition of normalized expression (*z*-score) levels of selected genes for each sample. (**I**) Enrichment of genes putatively regulated by both poised and de novo enhancers within KEGG and Reactome curated gene sets. MAPK, mitogen-activated protein kinase; PD-L1, programmed death-ligand 1.

examine whether Lin28b is associated with chromatin remodeling and innate programming in adult CD8$^+$ T cells, we performed ATAC-seq on CD8$^+$ T cells from adult Lin28b transgenic mice after bystander activation. Lin28b induction in adult cells permitted them to remodel their chromatin more rapidly after stimulation with innate cytokines, akin to neonatal cells (fig. S6, C to E). Because Lin28b specifies innate functions in lymphocytes (*17*), we asked whether the chromatin landscapes of neonatal and Lin28b cells overlapped with innate-like lymphocytes. We found that, under basal conditions (IL-2), neonatal and Lin28b cells resembled both adaptive (conventional CD4$^+$ and CD8$^+$ T cells) and innate-like lymphocytes (γδT cells and invariant NK T cells) (fig. S6C). However, after stimulation with innate cytokines, the neonatal and Lin28b cells lost their resemblance to conventional CD4$^+$ and CD8$^+$ T cells and displayed increased accessibility at loci that typify ILCs and NK cells (fig. S6C).

Neonatal CD8$^+$ T cells use a distinct set of TFs during bystander activation

Given that neonatal CD8$^+$ T cells displayed a marked increase in chromatin accessibility and expression of innate-like genes upon bystander activation, we sought to identify putative TFs that may bind to the open chromatin and regulate the expression of nearby genes (*36*, *37*). Because only certain CD8$^+$ T cell subsets deploy a robust bystander response, we performed single-cell ATAC-seq (scATAC-seq) to identify such TFs (Fig. 5A). We first identified distinct subsets of neonatal and adult cells exhibiting similar chromatin accessibility profiles; identified subsets were robust to the clustering approach used (Fig. 5B and fig. S7, A to C). We then projected each bystander-stimulated subset onto a single PCA plot (Fig. 5C). This analysis allowed us to identify four groups with concordant chromatin accessibility profiles across multiple genes, reminiscent of the groups discriminated by scRNA-seq (Fig. 3, C and D).

To distinguish and annotate the groups, we performed GSEA on the PC1 loadings, revealing a strong association with virtual memory and fetal progenitor gene signatures (Fig. 5C). We then calculated gene set signature scores for each subset and identified genes uniquely accessible in each group (Fig. 5D and fig. S8A). These analyses showed that group i subsets had the highest innateness scores and the strongest accessibility for *Cd44* and multiple cytokines, including *Ifng*, *Csf2*, *Gzma*, *Il10*, *Il17f*, and *Il22* (Fig. 5D and fig. S8A). This group included three neonatal subsets (N0, N1, and N4; 60% of the neonatal cells) together with a single adult subset (A5; 6% of the adult cells), which corresponded to the fetal-derived adult subset from the scRNA-seq data (after integration of scRNA-seq and scATAC-seq, 92% of scATAC-A5 cells matched with scRNA-A5; fig. S8B). Therefore, group i corresponds to fetal-derived virtual memory-like cells, which exhibit the strongest bystander activation (Fig. 5D and fig. S8, C and D). Group iv displays the strongest true naïve and adaptiveness signatures and a lack of accessibility at the loci encoding cytokines associated with the neonatal bystander response (Fig. 5D and fig. S8, C and D). Thus, group iv represents true naïve-like cell subsets in neonates and adults. Groups ii and iii display gene activities and signatures intermediary between groups i and iv. Plotting both control and bystander activated subsets onto the same UMAP and PCA projections highlighted the differential activation between group i and group iv subsets (fig. S8, C and D).

To predict the TFs that may bind to the open chromatin in phenotypically similar subsets of cells, we identified marker peaks (preferentially open chromatin regions) for each subset and calculated enrichment of TF binding motifs within these regions (Fig. 5, E and F). The binding motifs for T-box and Runx families of factors were enriched in the regions specifically associated with fetal-derived virtual memory subsets (group i), consistent with prior reports (Fig. 5F) (*13*). We found enrichment for many bZip family factors, including Bach2 and AP-1 factors, which play key roles in TCR-mediated activation of CD8$^+$ T cells (*38*). These results were recapitulated by analyses using all accessible regions or marker peaks considering both control and bystander stimulated subsets (fig. S9, A and B). We also observed enrichment for SMARCC1, a component of the switch/sucrose nonfermentable (SWI/SNF) chromatin remodeling complex (*39*). Conversely, the group iv subsets displayed enrichment for Irf family factors, which dampen CD8$^+$ T cell activation (*40*), and Tcf7 family factors, which promote quiescence in naïve cells (*41*). Although signal transducer and activator of transcription 4 (STAT4) and NF-κB act downstream of IL-12 and IL-18 signaling, respectively, their binding motifs displayed similar accessibility across both adult and neonatal activated subsets (fig. S9C), suggesting that they may be regulated via mechanisms other than binding accessibility.

TF binding motif enrichment alone does not uncover the gene expression programs regulated by enriched TFs. Therefore, we investigated whether these TF families facilitate the up-regulation of genes whose increased expression underlies neonatal bystander activation. To link the distinct chromatin accessibility and gene expression profiles of bystander activated neonatal subsets, we integrated our scRNA-seq and scATAC-seq datasets to map single-cell expression and chromatin accessibility profiles. After integration, we identified thousands of putative enhancers, each correlated ($r^2 > 0.70$) to gene expression changes (fig. S10A). This analysis defined a set of putative enhancers distinct to group i subsets that contained bZip binding motifs and were associated with expression of cytokine and effector protein genes, including *Ifng*, *Csf2*, *Il13*, *Il22*, *Tnfrsf8/9/11*, and *Il2rb* (fig. S10, B and C). For example, chromatin regions predicted to regulate *Csf2* expression contain binding motifs of bZip family TFs and are most accessible in group i subsets, which express the highest levels of *Csf2* mRNA (Fig. 5G). These results suggest that the bZip family of TFs play key roles during the bystander activation of neonatal CD8$^+$ T cells.

The Bach2/AP-1 axis specifies CD8$^+$ T cell innateness

Within the bZip family, the roles of Bach2 and AP-1 have been studied in CD8$^+$ T cells after antigenic stimulation, but their involvement in bystander activation has remained largely unexplored. In response to TCR stimulation, AP-1 TFs bind to enhancers of multiple genes that promote effector differentiation, whereas Bach2 serves as a transcriptional repressor and limits effector cell differentiation by competing with AP-1 TFs at shared binding sites (*38*, *42*). Thus, we hypothesized that neonatal CD8$^+$ T cells undergo robust bystander activation because they express lower amounts of Bach2, resulting in increased binding by AP-1 TFs upon stimulation with innate cytokines (Fig. 6A).

To test our hypothesis, we asked whether AP-1 TFs become bound in neonatal CD8$^+$ T cells upon stimulation with innate cytokines. This question was important because the scATAC-seq analysis of TF usage was based on the enrichment of TF motifs in open regions of chromatin; however, such enrichment does not provide direct evidence of TF activity. To reliably detect TF activity in CD8$^+$ T cells after bystander activation, we performed TF footprinting analysis (inferring TF binding) using the Bivariate Genomic

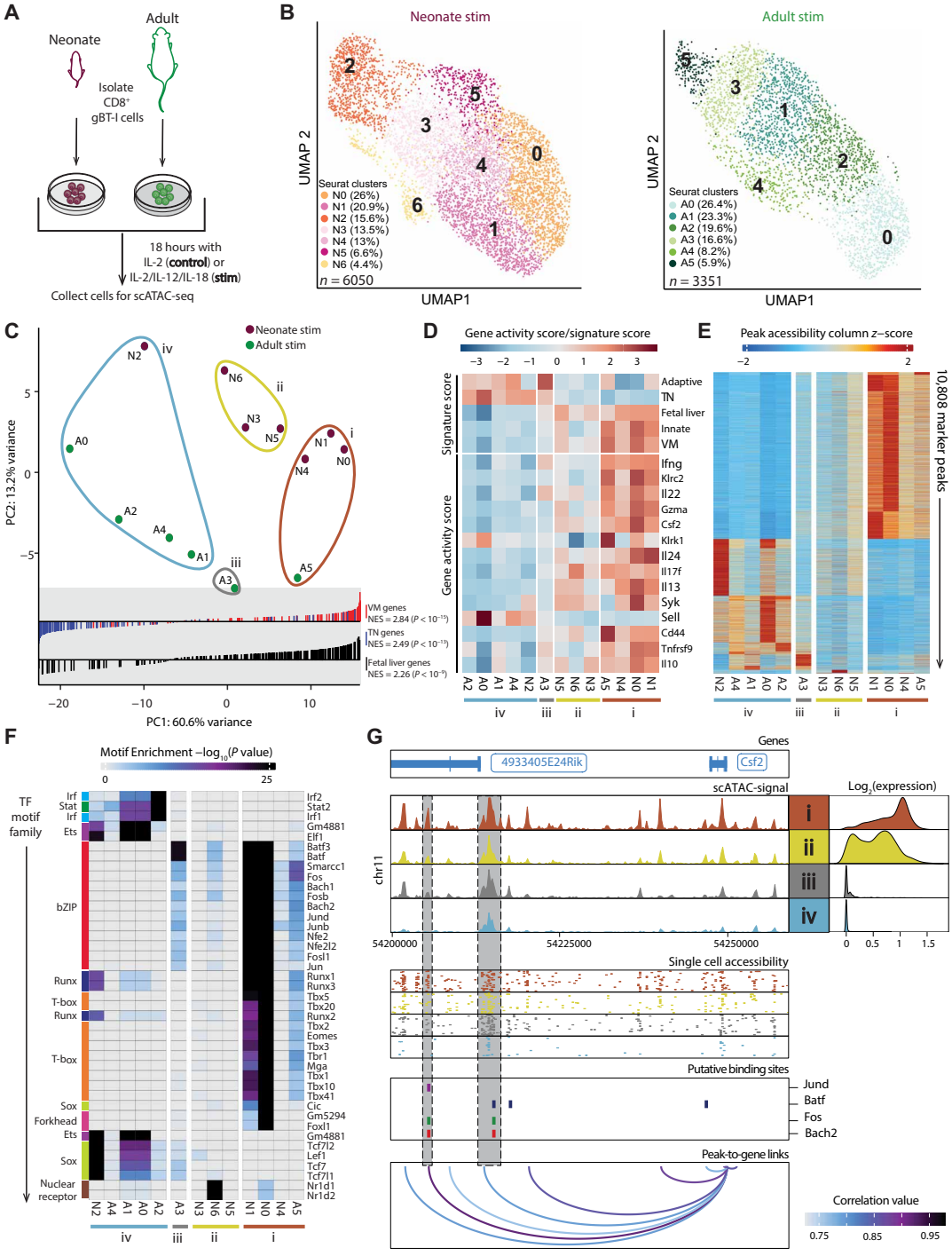

Fig. 5. Neonatal CD8$^+$ T cell subsets use a distinct set of TFs during bystander activation. (**A**) Neonate (cell $n = 6050$) and adult (cell $n = 3351$) CD8$^+$ T cells were stimulated overnight with IL-2 ± IL-12/18, and live CD8$^+$ T cells were sorted for scATAC-seq ($n = 1$; for neonates, three or four mice were pooled). (**B**) UMAP visualization of scATAC-seq data from neonate (left) and adult (right) cells after IL-12/18 stimulation with subset identities overlaid using labels and different colors; the proportion of the total sample is shown for each subset in parentheses. (**C**) PCA plot of pseudo-bulk gene accessibility profiles of subsets from (B); subsets with similar gene accessibility profiles are assigned a group number (i to iv). Above the *x* axis, GSEA gene rank plots depict the enrichment of virtual memory (red), true naïve (blue), and fetal-liver (black) gene sets among genes with positive, negative, and positive PC1 loadings, respectively. NES and adjusted *P* values are indicated. (**D**) Row-scaled gene set signature scores and gene activity scores of noteworthy effector molecules and phenotypic markers derived from pseudo-bulk gene accessibility profiles of subsets. Subsets are ordered by the groups corresponding to (C). (**E**) Column-scaled accessibility at 10,808 marker peaks (columns) across all subsets. (**F**) TF binding motif enrichment within the marker peaks of each subset; heatmap color indicates the enrichment *P* value ($-\log_{10}$). TF motif families are indicated by colored bars at the bottom. The heatmap rows correspond to scATAC-seq subsets and are ordered by the groups corresponding to (C). (**G**) Example data showing a genome browser view depicting aggregated and single-cell chromatin accessibility, putative TF binding sites, peak-to-gene links, and integrated scRNA-seq expression at the *Csf2* locus.

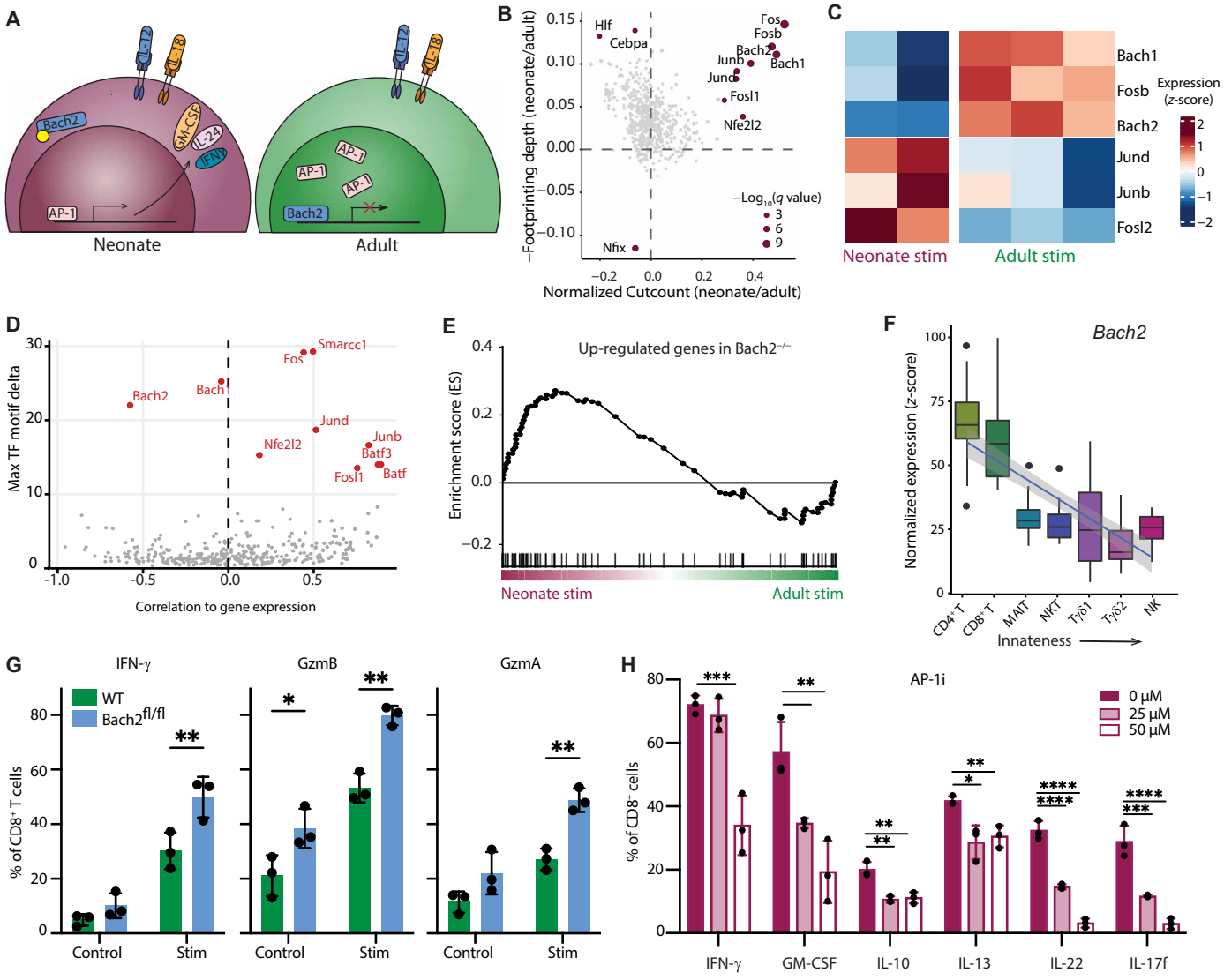

Fig. 6. The AP-1/Bach2 axis regulates innateness of CD8$^+$T cells. (**A**) Depiction of hypothesized Bach2 and AP-1 interplay during IL-12/18 stimulation of neonatal and adult CD8$^+$ T cells. (**B**) Scatter plots showing changes in flanking chromatin accessibility (*x* axis) and in footprinting depth (*y* axis) at predicted binding sites of different TFs between neonate and adult CD8$^+$ T cells after IL-12/18 stimulation. Dots represent TFs, and dot sizes indicate chi-square *q* values representing significance of change in either flanking accessibility or footprinting depth. TFs with significant changes are labeled, and the TFs without any significant changes are colored in gray. (**C**) Heatmap visualization of row-scaled gene expression of *Bach*, *Jun*, and *Fos* TF members with significant change between neonates and adult. (**D**) Scatter plot correlating the level of expression and binding motif accessibility of TFs across all single cells (*x* axis) while depicting magnitude of variability in the accessibility of each TF's cognate binding motif across all single cells (*y* axis). (**E**) GSEA showing that genes up-regulated in *Bach2*$^{-/-}$ CD8$^+$ T cells are also up-regulated in neonatal cells after IL-12/18 stimulation. (**F**) Distributions of normalized expression (*z*-scores) of *Bach2* across replicates in various human immune cells (GSE124731) (*x* axis) arranged in increasing order of their innateness potential. (**G**) Bystander response compared between adult WT and *Bach2*$^{fl/fl}$ mice CD8$^+$ T cells. Tat-cre was used to excise Bach2 in vitro. Statistical significance determined by ordinary two-way ANOVA followed by Šidák's multiple comparison test. (**H**) Percentages of live CD8$^+$ T cells expressing different cytokines after IL-12/18 stimulation in neonatal cells treated with increasing concentrations of the AP-1 inhibitor SR 11302. Significant differences compared to control (0 μM) were determined by one-way ANOVA followed by Dunnett's multiple comparisons test. For statistical comparisons, *$P < 0.05$, **$P < 0.01$, ***$P < 0.001$, and ****$P < 0.0001$.

Footprinting (BaGFoot) algorithm (*43*), which considers both footprinting and motif-flanking accessibility to infer TF activity. We performed this analysis with our bulk ATAC-seq dataset because the increased resolution available in conventional ATAC-seq data is better suited to BaGFoot. Under basal conditions, the neonatal cells exhibited increased footprints and flanking accessibility for the T-box family of TFs [T-bet (*Tbx*) and *Eomes*], consistent with previous studies (fig. S11A) (*13*). However, after stimulation, the family of TFs that exhibited the largest footprints and flanking accessibility corresponded to *Bach2* and the AP-1–related TFs (e.g., *Fos* and *Jun*), suggesting that these TFs are bound in neonatal cells after stimulation with innate cytokines (Fig. 6B).

Because Bach2 and AP-1–related TFs bind to the same TF binding motif, the footprinting data cannot reveal which TF is preferentially used by neonatal CD8$^+$ T cells during bystander activation. Thus, we examined *Bach2* and AP-1 expression levels. We found that many of the AP-1–related TFs were more highly expressed in neonatal cells (e.g., *Jund*, *Junb*, and *Fosl2*), whereas *Bach2* was more highly

expressed in adult cells (Fig. 6C). These analyses imply that neonatal cells exhibit both heightened AP-1 TF expression and heightened chromatin accessibility at AP-1 binding motifs, thereby enabling their activity. To validate this implication, we used our integrated single-cell datasets to demonstrate that AP-1 TF expression was correlated with the accessibility of their binding motifs at single-cell resolution (Fig. 6D). In addition, *Bach2* expression was negatively correlated with the accessibility of its binding motifs (Fig. 6D). These observations imply that decreased *Bach2* expression in neonates potentiates occupation of accessible chromatin by AP-1 TFs. In contrast, elevated *Bach2* expression in adult cells precludes binding of AP-1 TFs.

To explore the functional impact of *Bach2* loss, we reexamined data from an earlier study. Genes up-regulated in *Bach2*$^{-/-}$ CD8$^+$ T cells (*38*) were also up-regulated in neonatal cells after innate cytokine stimulation, implicating a role for *Bach2* in bystander activation of CD8$^+$ T cells (Fig. 6E). We also examined *Bach2* expression across other lymphocytes (*16*) and found that its expression was reduced in innate-like lineages of cells capable of undergoing bystander activation and up-regulated in conventional, adaptive T cells (Fig. 6F). Thus, expression of *Bach2* is inversely correlated with the "innateness" of T cells.

To obtain direct evidence that the AP-1/Bach2 axis regulates innate functions in CD8$^+$ T cells, we crossed floxed *Bach2* mice (*44*) to gBT-I mice and examined whether adult cells could be made more responsive to innate cytokines by deleting *Bach2*. To avoid any complications from inhibiting expression of *Bach2* during early stages of T cell development, we cultured peripheral mature CD8$^+$ T cells from adult *Bach2*$^{fl/fl}$ mice with tat-cre fusion protein. A higher percentage of adult cells produced IFN-γ, gzmB, and gzmA when *Bach2* was deleted (Fig. 6G). Thus, a role of Bach2 in adult CD8$^+$ T cells is to preclude their ability to respond to innate cytokines. To complement these experiments, we treated neonatal CD8$^+$ T cells with a chemical inhibitor of AP-1 (AP-1i) before stimulation with IL-12 and IL-18 (Fig. 6H). The dampening of AP-1 activity in neonatal cells led to a strong reduction in the production of cytokines. Together, these data suggest that CD8$^+$ T cells use the Bach2/AP-1 axis to tune innate responsiveness.

Innateness is conserved in human CD8$^+$ T cells

To address whether similar patterns of innateness are observed in human CD8$^+$ T cells, we performed scRNA-seq on human cord blood CD8$^+$ T cells from fetal (24 to 26 weeks after conception), neonatal (>37 weeks after conception), and adult (23 to 32 years of life) individuals after bystander activation (Fig. 7A and fig. S12, A and B). Consistent with our findings in mice, human cells produced in early life exhibited a more "inflammation-responsive" phenotype, as evidenced by their enhanced ability to up-regulate *IFNG* after innate cytokine stimulation (Fig. 7B). We also observed substantial variability in *IFNG* gene expression across the fetal and neonatal CD8$^+$ T cell pool (Fig. 7B). To better understand this cell-to-cell variability, we performed clustering analysis on each age group (Fig. 7C), which revealed distinct subsets of cells expressing unique surface receptors and effector molecules (Fig. 7D and fig. S12C). After projecting the expression profiles of all subsets onto a single PCA, we observed different groups of CD8$^+$ T cells from each age group with similar patterns of gene expression (Fig. 7E). Similar to our mouse data, we identified multiple subsets of fetal (F4 and F6) and neonatal (N3 and N4) human CD8$^+$ T cells that were highly enriched for innateness genes (Fig. 7F, groups I to II).

We also observed a single cluster of cells in adults (A5; 3.2% of adult cells) that was highly responsive to inflammation. This subset did not express *ZBTB16* (PLZF, a marker for unconventional T cells such as NKT and MAIT cells) and was most like subsets of human CD8$^+$ T cells found in fetal (F6) and neonatal samples (N4; group II), suggesting that this cluster represents fetal-derived CD8$^+$ T cells that persist into adulthood. Last, we examined whether key TF usage by innate and adaptive subsets of CD8$^+$ T cells was conserved. We found that the inflammation-responsive subsets of human cells exhibited reduced *BACH2* and higher *JUND* expression (Fig. 7G). Together, these observations indicate that the mouse and human CD8$^+$ T cell compartments have a similar developmental architecture and that the roles of the TFs that specify innateness and adaptiveness in the CD8$^+$ T cell pool are likely conserved.

DISCUSSION

An intriguing feature of neonatal lymphocytes is that they are highly responsive to inflammation and can rapidly produce a wide variety of cytokines. For example, subsets of γδT cells in neonatal mice secrete IFN-γ and IL-4 or IL-17 upon activation (*45*, *46*). There is also heterogeneity in the neonatal B1 B cell pool, with subsets producing IL-10 and others making GM-CSF and IL-3 (*47*, *48*). Here, we found a variety of distinct cytokine-producing subsets in the neonatal CD8$^+$ T cell pool after stimulation with innate cytokines. In this work, we show that neonatal CD8$^+$ T cells have greater functional diversity than adult CD8$^+$ T cells at both the individual cell and population level.

An interesting question is, why does the immune system require a more functionally diverse pool of neonatal CD8$^+$ T cells? In early life, the neonatal immune system must protect the host against a large swath of pathogens, and it must do so with a restricted set of T cells, which are also lacking in immunological memory (*8*, *49*). Thus, it is likely beneficial for the neonatal T cell pool to be highly responsive to inflammation and quickly generate a variety of cytokines and effector molecules, in hopes that the cost of making some unnecessary cytokines is outweighed by the benefit of making a variety of cytokines that could potentially be useful against diverse pathogens. However, as the frequency of unexperienced infections decreases and the diversity of the T cell pool increases, it likely becomes less advantageous for the host to use this bet-hedging immune strategy (*50*) and more necessary for a more controlled and antigen-specific pathogen response.

Perhaps one of the most unexpected findings from our study is that neonatal CD8$^+$ T cells are more responsive to inflammation than adults because of their ability to undergo chromatin remodeling. Earlier studies have demonstrated that CD8$^+$ T cells undergo extensive chromatin remodeling after antigenic stimulation, clonal expansion, and differentiation (*51*, *52*). However, we observed notable changes in the epigenomes of neonatal cells after brief stimulation with innate cytokines alone. The appearance of de novo enhancers in neonatal cells after stimulation matches previous findings in macrophages (*34*) and NK cells (*35*). For example, the "latent," or de novo, enhancers induced in neonatal CD8$^+$ T cells, macrophages, and NK cells are enriched in AP-1 sites, which may correspond to the reported chromatin modifying activity of AP-1 itself (*53*, *54*) or STATs (*35*, *55*). These data suggest that responsiveness by innate-like lymphocytes derives from both increased chromatin accessibility in the resting state and their ability to rapidly alter the preexisting chromatin structure in response to stimulation.

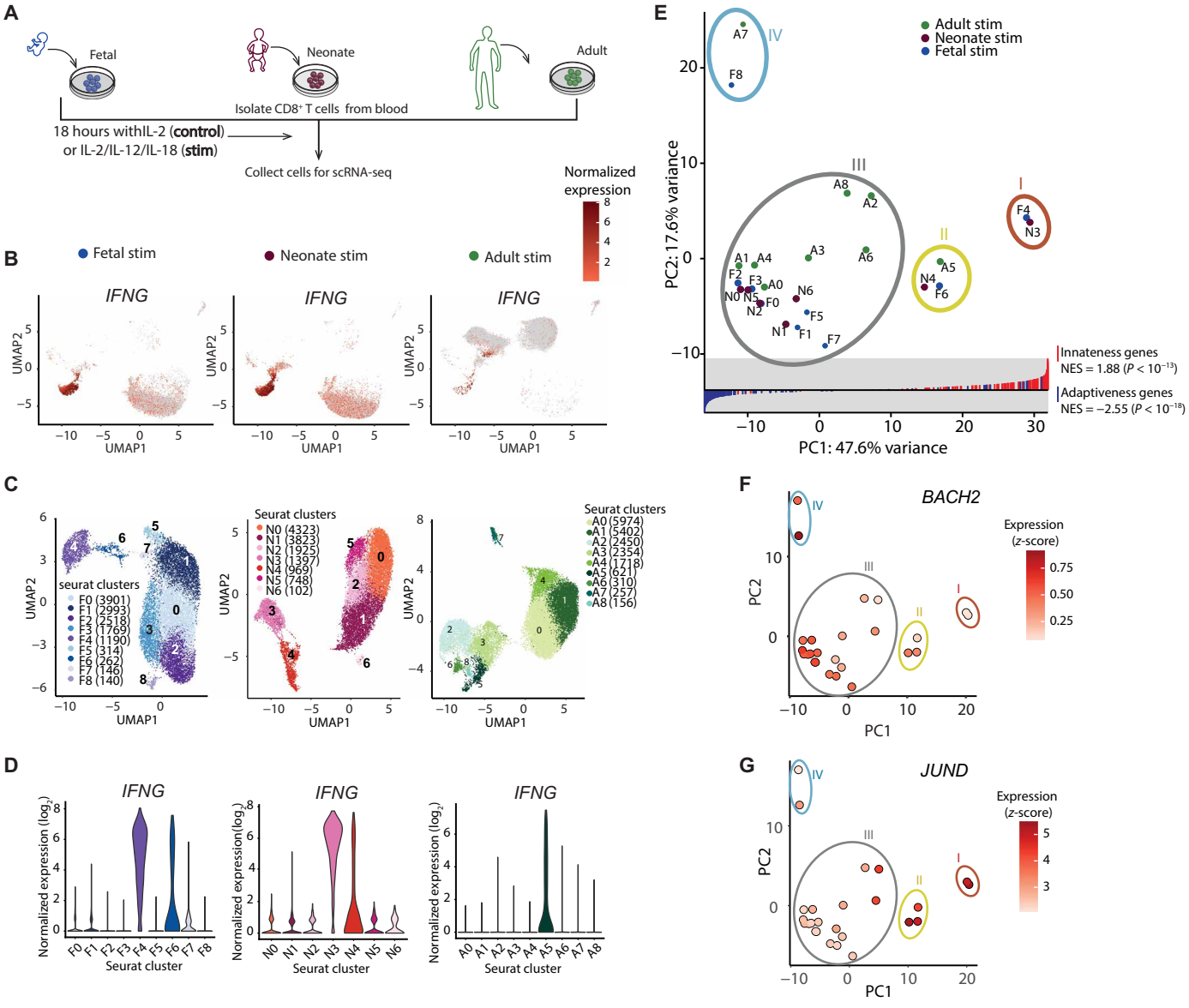

Fig. 7. Innateness profiles of different-aged CD8$^+$ T cells are conserved in humans. (**A**) Human CD8$^+$ T cells were isolated from adult PBMCs, neonate, or fetal CBMCs and stimulated overnight with IL-2 ± IL-12/18. (**B**) UMAP comprising scRNA-seq data from the entire cohort (see fig. S7A) divided into different age groups after stimulation [adult, $n = 4$ (2 males and 2 females); neonate, $n = 3$ (1 male and 2 females); and fetal, $n = 4$ (2 males and 2 females), cells from each cohort pooled]. Each UMAP is colored by the single-cell levels of *IFNG*. (**C**) UMAP representation of adult (left), neonatal (middle), and fetal (right) samples after IL-12/18 stimulation with cluster identifies overlaid using labels and different colors. (**D**) Expression of *IFNG* in each cluster of cells from (C). (**E**) PCA plot of pseudo-bulk gene expression profiles of subsets from (C); subsets with similar gene expression profiles are assigned a group number (I to IV). GSEA gene rank plots (inset) depict the enrichment of innateness (red) and adaptiveness (blue) gene sets among genes with positive and negative PC1 loadings, respectively, along the *x* axis. NES and adjusted *P* values are indicated. (**F** and **G**) PCA plot from E displaying corresponding z-score expression of *BACH2* (F) and *JUND* (G) for each Seurat cluster.

The ability of neonatal CD8$^+$ T cells to respond to inflammation and undergo bystander activation also relates to a reduction in Bach2, a transcriptional repressor that serves as a "placeholder" for the AP-1 family of TFs (*38*). Lower Bach2 levels in neonatal CD8$^+$ T cells likely increase the probability that the activation threshold will be reached upon bystander stimulation. That is, genes whose activation is precluded by Bach2 occupancy in adults are rendered responsive in neonates. In contrast, adult CD8$^+$ T cells exhibit elevated levels of Bach2, which suppresses their ability to become activated by innate cytokines. Thus, although adult cells are less capable of providing innate immune protection, their higher levels of Bach2 likely allows them to efficiently form memory cells after antigenic stimulation. Previous work has shown that Bach2 limits terminal differentiation of effector CD8$^+$ T cells after TCR stimulation by blocking access of AP-1 (*38*). Therefore, the AP-1/Bach2 axis appears to serve as a switch and specifies innate functions (inflammation responsiveness) or adaptive properties (memory development) of peripheral CD8$^+$ T cells at various stages of life.

Our data offers support for the layered immune model of development, in both mice and humans. At present, the prevailing

notion is that the naïve $CD8^+$ T cell pool is homogenous and that the change in "average phenotype" at different stages of life comes from a maturation of individual cells along a linear axis. However, we show that the $CD8^+$ T cell pool is far more diverse than previously recognized, comprising classical adaptive cells together with a complex population of more innate cells. Moreover, the shift from innateness to adaptiveness is mediated by developmental-related changes in the abundance of functionally distinct subpopulations of cells. By viewing these subsets as "building blocks," we may be able to understand how the structure of the $CD8^+$ T cell compartment changes with progressing development and ultimately sets the rheostat for responsiveness in adulthood.

In the future, it would be informative to investigate how permanent the chromatin changes are in neonatal $CD8^+$ T cells, how chromatin remodeling differs in antigen-experienced versus virtual memory cells, and whether $CD8^+$ T cells in early life can undergo a form of "trained immunity," akin to macrophages. It would also be useful to study the innate-like $CD8^+$ T cell subset found in humans and understand how environmental factors and host genetics alter the innate functions of $CD8^+$ T cells. Last, it will be important to determine how neonatal $CD8^+$ T cells interact with other types of immune cells to provide innate defense. Such studies will broaden our fundamental understanding of immune development and the mechanisms that regulate innate and adaptive functions.

MATERIALS AND METHODS

Study design

We investigated the bystander activation program in $CD8^+$ T cells, using flow cytometry and multi-omics to determine how $CD8^+$ T cells from different aged mice respond to innate cytokines and infection experiments to demonstrate relevance. We used single-cell genomics to characterize the heterogeneity of the bystander response and to identify the underlying gene regulatory mechanisms and validated these findings in mice. All experiments were repeated at least twice unless otherwise stated. Samples sizes and statistical tests are indicated in the figure legends.

Mice

TCR transgenic mice specific for the HSV-1 glycoprotein $B_{498–505}$ peptide SSIEFARL (gBT-I mice) (*56*) were provided by J. Nikolich-Zugich (University of Arizona, Tucson, AZ) and crossed with C57BL/6 or Thy1.1 mice (Charles River Laboratories, Wilmington, MA; and Jackson Laboratory, Bar Harbor, ME, respectively). Neonate (5 to 7 days) and adult (2 to 4 months) gBT-I animals were used. $TCRa^{-/-}$ recipients were purchased from the Jackson Laboratory. Bach2 fl/fl mice (*44*) were provided by W. Yokoyama (Washington University, St. Louis, MO) and crossed to gBT-I mice. Female mice were used for in vitro bystander and influenza experiments, and male mice were used for *L. monocytogenes* and *N. brasiliensis* experiments. Mice were maintained under specific pathogen–free conditions at Cornell University College of Veterinary Medicine, accredited by Association for Assessment and Accreditation of Laboratory Animal Care. Protocols were approved by the Institutional Animal Care and Use Committee at Cornell University.

Human samples

Frozen de-identified male and female preterm cord blood (24 to 29 weeks; fetal), full-term cord blood (39 to 41 weeks; neonatal), or adult (23 to 32 years) peripheral blood mononuclear cells (CBMCs or PBMCs, respectively) were obtained from the Biorepository Core at the University of Rochester. All study procedures were approved by the University of Rochester Medical Center Internal Review Board (protocol nos. RPRC00045470 and 37933), and all individuals' caregivers provided informed consent. Individuals were excluded for known congenital anomalies or genetic disorders present or suspected, individual nonviability, and for maternal HIV or inherited disorders known to affect immune development. Samples were de-identified before shipping to Cornell. Frozen CMBCs and PBMCs were quick thawed and rested overnight in RPMI 1640 with 10% fetal bovine serum (RP-10) at 37°C.

Flow cytometry

Antibodies were purchased from Thermo Fisher Scientific (Waltham, MA), BioLegend, or BD Biosciences (San Jose, CA). A list of antibodies used can be found in table S1. For intracellular staining, the FIX & PERM Cell Permeabilization Kit from Thermo Fisher Scientific was used, and data were collected (FACSSymphony; BD Biosciences) and analyzed (FlowJo; BD Biosciences). To purify live gBT-I Tg adult, neonate, and Lin28b $CD8^+$ T cells for bulk RNA-seq, ATAC-seq, and scRNA-seq after bystander activation, live $CD8^+$ $V\beta8^+$ cells were fluorescence-activated cell sorting (FACS)–sorted to >95% purity with a FACSAria Fusion Sorter (BD Biosciences). For human scRNA-seq experiments live $CD235a^-$ $CD4^-$ $CD8^+$ cells were FACS-sorted to >96% purity after bystander activation. Antibody clones used are CD235a [HIR2 (GA-R2)], CD4 (RPA-T4), and CD8 (RPA-T-8).

In vitro bystander activation

Single-cell suspensions from the spleen were obtained by manual dissociation, and $CD8^+$ T cells were isolated by positive magnetic separation using anti-CD8a microbeads (Miltenyi Biotec). $CD8^+$ T cells (2×10^5) were plated per well and incubated in RP-10 with recombinant human IL-2 (10 ng/ml; Thermo Fisher Scientific) for 18 to 22 hours. For bystander-activated samples, medium was supplemented with recombinant murine IL-12p70 and IL-18 (Thermo Fisher Scientific) at 1 ng/ml unless specified. Brefeldin A (1.5 mg/ml; MilliporeSigma, St. Louis, MO) was added for the final 4 hours of incubation before antibody labeling for flow cytometry analysis, or cells were immediately labeled for FACS sorting. Cells activated with IL-2/IL-12/IL-18 together are referred to as the stim group, whereas those cultured with IL-2 alone are referred to as the control group. For human cells, $CD8^+$ cells were magnetically enriched by positive selection (anti-human CD8 microbeads; Miltenyi Biotech) from rested PBMCs or CBMCs and subjected to bystander activation as described above using RP-10 supplemented with recombinant human IL-2, IL-12p70, and IL-18 at 10 ng/ml (BioLegend, San Diego, CA).

Tat-cre deletion of Bach2

Magnetically enriched $CD8^+$ T cells from Bach2 fl/fl gBT-I or Bach2 wt/wt gBT-I mice were treated for 4 hours with 250 mM Tat-cre (MilliporeSigma) in RP-10. Cells were washed, resuspended in RP-10 containing IL-7 (10 ng/ml), and incubated for 72 to 96 hours before cytokine stimulation.

AP-1 inhibitor experiments

Enriched murine splenic $CD8^+$ T cells were pretreated for 1 hour at 37°C with RP-10 supplemented with recombinant human IL-2 (10 ng/ml) and either dimethyl sulfoxide (DMSO) or SR 11302 AP-1 inhibitor (AP-1i, Tocris Bio-Techne, Minneapolis, MN) at the indicated concentrations. Cells were pelleted and resuspended in RP-10

containing IL-2 with or without IL-12 (1 ng/ml) and IL-18 (1 ng/ml) in the presence of DMSO or AP-1i for 18 to 22 hours.

In vivo infections

$CD8^+$ T cells from gBT-I adult, neonate, or Lin28b mice were magnetically enriched using anti-CD8a microbeads (Miltenyi). Cells were labeled with antibodies against CD8, Vα2, and Vβ8, and flow cytometry was performed to determine the percentage of gBT-I $CD8^+$ T cells ($V\alpha2^+V\beta8^+$). gBT-I cells (3×10^5) in phosphate-buffered saline (PBS) were intravenously injected into adult $TCRa^{-/-}$ or juvenile B6 (2 weeks of age) recipients. The next day recipients were infected with WT *L. monocytogenes*, WT influenza A virus, or WT *N. brasiliensis*. WT *L. monocytogenes* (*L. monocytogenes*, strain 10403) was obtained from J. Nikolch-Zugich (University of Arizona), and bacterial burden in the liver was quantified at day 3 after intravenous infection with 1×10^4 colony-forming units as described (*57*). WT Prg/A/PR/8/34 (H1N1) influenza was provided by J. Boon (Washington University). Mice were injected intranasally with 100 median tissue culture infectious dose in 50 μl of PBS and weighed daily. At 7 days postinfection (dpi), lungs were homogenized in Dulbecco's modified Eagle's medium supplemented with penicillin-streptomycin (GentleMACS dissociator). RNA was extracted (MagMAX Total Nucleic Acid Isolation Kit; Thermo Fisher Scientific) and Centers for Disease Control and Prevention (CDC) universal influenza A matrix gene qPCR assay (*58*) performed on the 7500 Fast Real-Time PCR System (Thermo Fisher Scientific). For *N. brasiliensis* infections, larvae maintained as previously described (*59*) were used. Mice were infected subcutaneously (subQ) with 500 L3 larvae in PBS. At 10 dpi, small intestines were harvested, and adult worms quantified from intestinal tissues as described (*59*).

RNA-seq

RNA-seq data analysis

Differential expression analysis was performed using edgeR (*60*). Genes with more than 1 count per million (CPM) in at least two samples were retained. PCA was performed using log-transformed CPM values with pseudo-count of 0.1 (prcomp, in R). GSEA was performed by fgsea against Kyoto Encyclopedia of Genes and Genomes (KEGG) and Hallmark gene sets.

Innateness score calculation

The genes associated with human innateness or adaptiveness were obtained from Gutierrez-Arcelus *et al.* (*16*). *Z*-scores of innateness and adaptiveness genes were multiplied by +1 and −1, respectively, and aggregated by summation into one value per sample (RNA-seq) or per cell (scRNA-seq) and referred to as an innateness score.

Assay for transposase-accessible chromatin using sequencing

ATAC-seq peak calling and visualization

The peaks of ATAC-seq reads were called using macs2 (parameters: -f BAMPE -g mm -B -q 0.05) [(*61*); https://github.com/macs3-project/MACS], and reproducible peaks were obtained using Irreproducibility Discovery Rate analysis (https://github.com/ENCODE-DCC/atac-seq-pipeline). The peaks from all samples were merged [bedtools; (*62*)] to generate a unified peak set. The accessibility at these peaks was estimated by counting the number of ATAC-seq reads that map to peak regions using featureCounts (*63*), and these counts were TMM-normalized (trimmed mean of M-values). The PCA analysis was performed using prcomp, and differential accessibility analysis was performed using edgeR (*60*). The ATAC-seq peaks were mapped to the nearest gene (bedtools) and classified into promoter-proximal or enhancer peaks based on proximity to the nearest transcription start site (TSS); the promoter region was defined as 1 kb upstream and 500 base pair (bp) downstream of a TSS. The innateness score was calculated in the same way as for RNA-seq, except that the counts for ATAC-seq peaks that map to the innateness and adaptiveness genes were used. For visualization, raw read counts per nucleotide were normalized by the total genome-mapped reads and converted to bigwig format using bedtools (bamToBed and genomeCoverageBed) and bedGraphToBigWig (*64*); bigwig files were visualized using UCSC genome browser (https://genome.ucsc.edu/). The analysis of de novo and poised enhancers is described in the Supplementary Materials. For TF footprinting analysis, we used BaGFoot to quantify flanking accessibility and footprinting depth for all TF motifs in CisBP database (*65*) and used chi-square tests to identify motifs with significant differences in flanking accessibility and/or TF footprinting (*43*).

Single-cell RNA-seq

Mouse scRNA-seq data analysis

We normalized, scaled, and regressed out variation in unique molecular identifier (UMI) counts and mitochondrial content; performed dimensionality reduction; and generated UMAP projections using Seurat v2.3.3. We used SAVER (*66*) to impute the data, which was used only for clustering and dimensionality reduction; downstream analyses were performed using original count data. For analysis of individual samples after stimulation, we used the imputed data for clustering (resolution of 0.6) and UMAP generation. Dot and violin plots were generated using the original normalized count data (Seurat). For PCA analysis, we generated pseudo-bulk expression profiles for each cluster using AverageExpression (Seurat), log-transformed the data, and generated PCA using the prcomp function. The innateness, fetal liver, and virtual memory/true naïve scores were calculated in same way as the bulk RNA-seq data. The fetal liver (*26*), true naïve, and virtual memory gene sets (*13*) were derived from the literature; GSEA was performed using fgsea comparing the gene sets against all expressed genes ranked by their PC loading values. Groups of subsets were defined manually considering the shared gene signature scores and expression profiles of pseudo-bulk subsets. Analyses were performed on individual subsets, not on multi-subset groupings.

Human scRNA-seq data analysis

The raw FASTQ data were processed using Cell Ranger v3.0.1, and the resulting count matrixes were filtered using Seurat v4.0.1 (*67*) to remove cell barcodes with less than 700 genes and with more than 15% mitochondrial counts. We produced high-quality data for 92,840 individual cells with an average of 15,473 cells per condition and 2174 genes and 7288 UMIs detected per cell. We normalized, scaled, and regressed out variation in mitochondrial content; performed dimensionality reduction; and generated UMAP projections using Seurat v.4.0.1. The calculation of innateness scores for single cells is described above in the bulk RNA-seq section. For analysis of individual conditions after stimulation, we used Harmony to normalize the data for interindividual differences and for projections (resolution of 0.2) and UMAP generations. Downstream analyses were performed in the same manner as the mouse data.

scATAC-seq library preparation and sequencing

scATAC-seq subset characterization

After quality filtering, cells were stratified by sample, and ArchR (*68*) was used for dimensionality reduction, subset formation, and

UMAP generation. Pseudo-bulk replicates were generated by sample, and MACS2 was implemented to create a union peak matrix composed of fixed-width 501-bp peaks. After peak calling, PCA was implemented (PCAtools) using gene activity scores as input. Innateness, adaptiveness, fetal-liver, virtual memory, and true naïve scores were calculated as outlined previously, replacing normalized read counts with gene activity scores. Heatmap visualization of gene signature and gene activity scores of effector molecules were preceded by *z*-score normalization across subsets. As with scRNA-seq data, scATAC-seq groups of subsets were defined considering the shared gene signature scores and accessibility profiles of pseudo-bulk subsets.

scATAC-seq analysis of marker features and TF motif enrichment

Gene activity scores were calculated using ArchR's gene score model, which heavily weights gene promoter (5 kb upstream of TSS) and gene body accessibility. Archr's getMarkerFeatures was used to identify marker peaks across all subsets using a false discovery rate cutoff (0.01) and a $\log_2$(fold-change) cutoff of 1.25. Enrichment testing of TF motifs within subset-specific marker peaks was performed by the peakAnnoEnrichment function of ArchR, using CIS-BP annotations (database versions 1.02-2.0). Enrichment testing of TF motifs within all accessible peaks was performed using monaLisa (*69*) using JASPAR 2022 annotations.

Statistical analysis

Statistical analyses (except for FlowSOM and sequencing, see above) were performed using Prism software (GraphPad, San Diego, CA), with significance determined by one-way or two-way analysis of variance (ANOVA) followed by a post hoc test, as indicated in the legends. Error bars represent SEM; significance is denoted as follows: $*P < 0.05$, $**P < 0.01$, $***P < 0.001$, and $****P < 0.0001$.

Supplementary Materials

This PDF file includes:
Methods
Figs. S1 to S12
Table S1
References (*70*–*80*)

Other Supplementary Material for this manuscript includes the following:
Data files S1 to S13
MDAR Reproducibility Checklist

REFERENCES AND NOTES

1. N. Zhang, M. J. Bevan, CD8$^+$ T cells: Foot soldiers of the immune system. *Immunity* **35**, 161–168 (2011).
2. M. A. Williams, M. J. Bevan, Effector and memory CTL differentiation. *Annu. Rev. Immunol.* **25**, 171–192 (2007).
3. S. M. Kaech, E. J. Wherry, R. Ahmed, Effector and memory T-cell differentiation: Implications for vaccine development. *Nat. Rev. Immunol.* **2**, 251–262 (2002).
4. J. T. White, E. W. Cross, M. A. Burchill, T. Danhorn, M. D. McCarter, H. R. Rosen, B. O'Connor, R. M. Kedl, Virtual memory T cells develop and mediate bystander protective immunity in an IL-15-dependent manner. *Nat. Commun.* **7**, 11291 (2016).
5. S. C. Jameson, Y. J. Lee, K. A. Hogquist, Innate memory T cells. *Adv. Immunol.* **126**, 173–213 (2015).
6. G. Lertmemongkolchai, G. Cai, C. A. Hunter, G. J. Bancroft, Bystander activation of CD8$^+$ T cells contributes to the rapid production of IFN-γ in response to bacterial pathogens. *J. Immunol.* **166**, 1097–1105 (2001).
7. H. Lee, S. Jeong, E. C. Shin, Significance of bystander T cell activation in microbial infection. *Nat. Immunol.* **23**, 13–22 (2022).
8. B. D. Rudd, Neonatal T cells: A Reinterpretation. *Annu. Rev. Immunol.* **38**, 229–247 (2020).
9. A. O. Galindo-Albarran, O. H. López-Portales, D. Y. Gutiérrez-Reyna, O. Rodríguez-Jorge, J. A. Sánchez-Villanueva, O. Ramírez-Pliego, A. Bergon, B. Loriod, H. Holota, J. Imbert, A. Hernández-Mendoza, P. Ferrier, E. C.-d. S. Pau, A. Valencia, S. Spicuglia, M. A. Santana, CD8$^+$ T cells from human neonates are biased toward an innate immune response. *Cell Rep.* **17**, 2151–2160 (2016).
10. C. Tabilas, J. Wang, X. Liu, J. W. Locasale, N. L. Smith, B. D. Rudd, Cutting edge: Elevated glycolytic metabolism limits the formation of memory CD8$^+$ T cells in early life. *J. Immunol.* **203**, 2571–2576 (2019).
11. N. L. Smith, E. Wissink, J. Wang, J. F. Pinello, M. P. Davenport, A. Grimson, B. D. Rudd, Rapid proliferation and differentiation impairs the development of memory CD8$^+$ T cells in early life. *J. Immunol.* **193**, 177–184 (2014).
12. B. D. Rudd, V. Venturi, M. P. Davenport, J. Nikolich-Zugich, Evolution of the antigen-specific CD8$^+$ TCR repertoire across the life span: Evidence for clonal homogenization of the old TCR repertoire. *J. Immunol.* **186**, 2056–2064 (2011).
13. N. L. Smith, R. K. Patel, A. Reynaldi, J. K. Grenier, J. Wang, N. B. Watson, K. Nzingha, K. J. Yee Mon, S. A. Peng, A. Grimson, M. P. Davenport, B. D. Rudd, Developmental origin governs CD8$^+$ T cell fate decisions during infection. *Cell* **174**, 117–130.e14 (2018).
14. J. Wang, E. M. Wissink, N. B. Watson, N. L. Smith, A. Grimson, B. D. Rudd, Fetal and adult progenitors give rise to unique populations of CD^{8+} T cells. *Blood* **128**, 3073–3082 (2016).
15. S. Bedoui, T. Gebhardt, G. Gasteiger, W. Kastenmuller, Parallels and differences between innate and adaptive lymphocytes. *Nat. Immunol.* **17**, 490–494 (2016).
16. M. Gutierrez-Arcelus, N. Teslovich, A. R. Mola, R. B. Polidoro, A. Nathan, H. Kim, S. Hannes, K. Slowikowski, G. F. M. Watts, I. Korsunsky, M. B. Brenner, S. Raychaudhuri, P. J. Brennan, Lymphocyte innateness defined by transcriptional states reflects a balance between proliferation and effector functions. *Nat. Commun.* **10**, 687 (2019).
17. J. Yuan, C. K. Nguyen, X. Liu, C. Kanellopoulou, S. A. Muljo, Lin28b reprograms adult bone marrow hematopoietic progenitors to mediate fetal-like lymphopoiesis. *Science* **335**, 1195–1200 (2012).
18. E. M. Wissink, N. L. Smith, R. Spektor, B. D. Rudd, A. Grimson, MicroRNAs and their targets are differentially regulated in adult and neonatal mouse CD8+ T cells. *Genetics* **201**, 1017–1030 (2015).
19. R. E. Berg, E. Crossley, S. Murray, J. Forman, Memory CD8+ T cells provide innate immune protection against *Listeria monocytogenes* in the absence of cognate antigen. *J. Exp. Med.* **198**, 1583–1593 (2003).
20. F. F. Huang, P. F. Barnes, Y. Feng, R. Donis, Z. C. Chroneos, S. Idell, T. Allen, D. R. Perez, J. A. Whitsett, K. Dunussi-Joannopoulos, H. Shams, GM-CSF in the lung protects against lethal influenza infection. *Am. J. Respir. Crit. Care Med.* **184**, 259–268 (2011).
21. G. J. McKenzie, A. Bancroft, R. K. Grencis, A. N. McKenzie, A distinct role for interleukin-13 in Th2-cell-mediated immune responses. *Curr. Biol.* **8**, 339–342 (1998).
22. C. Haluszczak, A. D. Akue, S. E. Hamilton, L. D. S. Johnson, L. Pujanauski, L. Teodorovic, S. C. Jameson, R. M. Kedl, The antigen-specific CD8$^+$ T cell repertoire in unimmunized mice includes memory phenotype cells bearing markers of homeostatic expansion. *J. Exp. Med.* **206**, 435–448 (2009).
23. A. D. Akue, J. Y. Lee, S. C. Jameson, Derivation and maintenance of virtual memory CD8 T cells. *J. Immunol.* **188**, 2516–2523 (2012).
24. A. Butler, P. Hoffman, P. Smibert, E. Papalexi, R. Satija, Integrating single-cell transcriptomic data across different conditions, technologies, and species. *Nat. Biotechnol.* **36**, 411–420 (2018).
25. L. A. Herzenberg, L. A. Herzenberg, Toward a layered immune system. *Cell* **59**, 953–954 (1989).
26. M. Oshima, N. Hasegawa, M. Mochizuki-Kashio, T. Muto, S. Miyagi, S. Koide, S. Yabata, G. R. Wendt, A. Saraya, C. Wang, K. Shimoda, Y. Suzuki, A. Iwama, Ezh2 regulates the Lin28/let-7 pathway to restrict activation of fetal gene signature in adult hematopoietic stem cells. *Exp. Hematol.* **44**, 282–296.e3 (2016).
27. S. McKinney-Freeman, P. Cahan, H. Li, S. A. Lacadie, H. T. Huang, M. Curran, S. Loewer, O. Naveiras, K. L. Kathrein, M. Konantz, E. M. Langdon, C. Lengerke, L. I. Zon, J. J. Collins, G. Q. Daley, The transcriptional landscape of hematopoietic stem cell ontogeny. *Cell Stem Cell* **11**, 701–714 (2012).
28. A. Reynaldi, N. L. Smith, T. E. Schlub, C. Tabilas, V. Venturi, B. D. Rudd, M. P. Davenport, Fate mapping reveals the age structure of the peripheral T cell compartment. *Proc. Natl. Acad. Sci. U.S.A.* **116**, 3974–3981 (2019).
29. Y. Li, W. Kong, W. Yang, R. M. Patel, E. B. Casey, T. Okeyo-Owuor, J. M. White, S. N. Porter, S. A. Morris, J. A. Magee, Single-cell analysis of neonatal HSC ontogeny reveals gradual and uncoordinated transcriptional reprogramming that begins before birth. *Cell Stem Cell* **27**, 732–747.e7 (2020).
30. E. V. Dang, J. Barbi, H.-Y. Yang, D. Jinasena, H. Yu, Y. Zheng, Z. Bordman, J. Fu, Y. Kim, H.-R. Yen, W. Luo, K. Zeller, L. Shimoda, S. L. Topalian, G. L. Semenza, C. V. Dang, D. M. Pardoll, F. Pan, Control of T(H)17/T(reg) balance by hypoxia-inducible factor 1. *Cell* **146**, 772–784 (2011).
31. S. Tanaka, A. Suto, T. Iwamoto, D. Kashiwakuma, S.-I. Kagami, K. Suzuki, H. Takatori, T. Tamachi, K. Hirose, A. Onodera, J. Suzuki, O. Ohara, M. Yamashita, T. Nakayama, H. Nakajima, Sox5 and c-Maf cooperatively induce Th17 cell differentiation via RORγt induction as downstream targets of Stat3. *J. Exp. Med.* **211**, 1857–1874 (2014).
32. C. A. Spinner, I. Lamsoul, A. Métais, C. Febrissy, C. Moog-Lutz, P. G. Lutz, The E3 ubiquitin ligase Asb2α in T helper 2 cells negatively regulates antitumor immunity in colorectal cancer. *Cancer Immunol. Res.* **7**, 1332–1344 (2019).

33. H.-Y. Shih, G. Sciumè, Y. Mikami, L. Guo, H.-W. Sun, S. R. Brooks, J. F. Urban Jr., F. P. Davis, Y. Kanno, J. J. O'Shea, Developmental acquisition of regulomes underlies innate lymphoid cell functionality. *Cell* **165**, 1120–1133 (2016).
34. R. Ostuni, V. Piccolo, I. Barozzi, S. Polletti, A. Termanini, S. Bonifacio, A. Curina, E. Prosperini, S. Ghisletti, G. Natoli, Latent enhancers activated by stimulation in differentiated cells. *Cell* **152**, 157–171 (2013).
35. G. Sciumè, Y. Mikami, D. Jankovic, H. Nagashima, A. V. Villarino, T. Morrison, C. Yao, S. Signorella, H.-W. Sun, S. R. Brooks, D. Fang, V. Sartorelli, S. Nakayamada, K. Hirahara, B. Zitti, F. P. Davis, Y. Kanno, J. J. O'Shea, H.-Y. Shih, Rapid enhancer remodeling and transcription factor repurposing enable high magnitude gene induction upon acute activation of NK cells. *Immunity* **53**, 745–758.e4 (2020).
36. G. Natoli, R. Ostuni, Adaptation and memory in immune responses. *Nat. Immunol.* **20**, 783–792 (2019).
37. N. Fernando, G. Sciumè, J. J. O'Shea, H.-Y. Shih, Multi-dimensional gene regulation in innate and adaptive lymphocytes: A view from regulomes. *Front. Immunol.* **12**, 655590 (2021).
38. R. Roychoudhuri, D. Clever, P. Li, Y. Wakabayashi, K. M. Quinn, C. A. Klebanoff, Y. Ji, M. Sukumar, R. L. Eil, Z. Yu, R. Spolski, D. C. Palmer, J. H. Pan, S. J. Patel, D. C. Macallan, G. Fabozzi, H.-Y. Shih, Y. Kanno, A. Muto, J. Zhu, L. Gattinoni, J. J. O'Shea, K. Okkenhaug, K. Igarashi, W. J. Leonard, N. P. Restifo, BACH2 regulates $CD8^+$ T cell differentiation by controlling access of AP-1 factors to enhancers. *Nat. Immunol.* **17**, 851–860 (2016).
39. J. Gatchalian, J. Liao, M. B. Maxwell, D. C. Hargreaves, Control of stimulus-dependent responses in macrophages by SWI/SNF chromatin remodeling complexes. *Trends Immunol.* **41**, 126–140 (2020).
40. S. Hida, K. Ogasawara, K. Sato, M. Abe, H. Takayanagi, T. Yokochi, T. Sato, S. Hirose, T. Shirai, S. Taki, T. Taniguchi, $CD8^+$ T cell-mediated skin disease in mice lacking IRF-2, the transcriptional attenuator of interferon-alpha/beta signaling. *Immunity* **13**, 643–655 (2000).
41. R. Kratchmarov, A. M. Magun, S. L. Reiner, TCF1 expression marks self-renewing human $CD8^+$ T cells. *Blood Adv.* **2**, 1685–1690 (2018).
42. G. Hu, J. Chen, A genome-wide regulatory network identifies key transcription factors for memory $CD8^+$ T-cell development. *Nat. Commun.* **4**, 2830 (2013).
43. S. Baek, I. Goldstein, G. L. Hager, Bivariate genomic footprinting detects changes in transcription factor activity. *Cell Rep.* **19**, 1710–1722 (2017).
44. K. Kometani, R. Nakagawa, R. Shinnakasu, T. Kaji, A. Rybouchkin, S. Moriyama, K. Furukawa, H. Koseki, T. Takemori, T. Kurosaki, Repression of the transcription factor Bach2 contributes to predisposition of IgG1 memory B cells toward plasma cell differentiation. *Immunity* **39**, 136–147 (2013).
45. C. E. Sutton, S. J. Lalor, C. M. Sweeney, C. F. Brereton, E. C. Lavelle, K. H. G. Mills, Interleukin-1 and IL-23 induce innate IL-17 production from gammadelta T cells, amplifying Th17 responses and autoimmunity. *Immunity* **31**, 331–341 (2009).
46. S. M. Hayes, R. M. Laird, P. E. Love, Beyond alphabeta/gammadelta lineage commitment: TCR signal strength regulates gammadelta T cell maturation and effector fate. *Semin. Immunol.* **22**, 247–251 (2010).
47. A. O'Garra, R. Chang, N. Go, R. Hastings, G. Haughton, M. Howard, Ly-1 B (B-1) cells are the main source of B cell-derived interleukin 10. *Eur. J. Immunol.* **22**, 711–717 (1992).
48. P. J. Rauch, A. Chudnovskiy, C. S. Robbins, G. F. Weber, M. Etzrodt, I. Hilgendorf, E. Tiglao, J. L. Figueiredo, Y. Iwamoto, I. Theurl, R. Gorbatov, M. T. Waring, A. T. Chicoine, M. Mouded, M. J. Pittet, M. Nahrendorf, R. Weissleder, F. K. Swirski, Innate response activator B cells protect against microbial sepsis. *Science* **335**, 597–601 (2012).
49. M. P. Davenport, N. L. Smith, B. D. Rudd, Building a T cell compartment: How immune cell development shapes function. *Nat. Rev. Immunol.* **20**, 499–506 (2020).
50. A. Mayer, T. Mora, O. Rivoire, A. M. Walczak, Diversity of immune strategies explained by adaptation to pathogen statistics. *Proc. Natl. Acad. Sci. U.S.A.* **113**, 8630–8635 (2016).
51. S. M. Gray, R. A. Amezquita, T. Guan, S. H. Kleinstein, S. M. Kaech, Polycomb repressive complex 2-mediated chromatin repression guides effector $CD8^+$ T cell terminal differentiation and loss of multipotency. *Immunity* **46**, 596–608 (2017).
52. B. Yu, K. Zhang, J. J. Milner, C. Toma, R. Chen, J. P. Scott-Browne, R. M. Pereira, S. Crotty, J. T. Chang, M. E. Pipkin, W. Wang, A. W. Goldrath, Epigenetic landscapes reveal transcription factors that regulate $CD8^+$ T cell differentiation. *Nat. Immunol.* **18**, 573–582 (2017).
53. S. C. Biddie, S. John, P. J. Sabo, R. E. Thurman, T. A. Johnson, R. L. Schiltz, T. B. Miranda, M. H. Sung, S. Trump, S. L. Lightman, C. Vinson, J. A. Stamatoyannopoulos, G. L. Hager, Transcription factor AP1 potentiates chromatin accessibility and glucocorticoid receptor binding. *Mol. Cell* **43**, 145–155 (2011).
54. M. Yukawa, S. Jagannathan, S. Vallabh, A. V. Kartashov, X. Chen, M. T. Weirauch, A. Barski, AP-1 activity induced by co-stimulation is required for chromatin opening during T cell activation. *J. Exp. Med.* **217**, e20182009 (2020).
55. G. Vahedi, H. Takahashi, S. Nakayamada, H.-W. Sun, V. Sartorelli, Y. Kanno, J. J. O'Shea, STATs shape the active enhancer landscape of T cell populations. *Cell* **151**, 981–993 (2012).
56. S. N. Mueller, W. Heath, J. D. McLain, F. R. Carbone, C. M. Jones, Characterization of two TCR transgenic mouse lines specific for herpes simplex virus. *Immunol. Cell Biol.* **80**, 156–163 (2002).
57. C. Tabilas, D. S. Iu, C. W. P. Daly, K. J. Yee Mon, A. Reynaldi, S. P. Wesnak, J. K. Grenier, M. P. Davenport, N. L. Smith, A. Grimson, B. D. Rudd, Early microbial exposure shapes adult immunity by altering CD8+ T cell development. *Proc. Natl. Acad. Sci. U.S.A.* **119**, e2212548119 (2022).
58. B. Shu, K.-H. Wu, S. Emery, J. Villanueva, R. Johnson, E. Guthrie, L. S. Berman, C. Warnes, N. Barnes, A. Klimov, S. Lindstrom, Design and performance of the CDC real-time reverse transcriptase PCR swine flu panel for detection of 2009 A (H1N1) pandemic influenza virus. *J. Clin. Microbiol.* **49**, 2614–2619 (2011).
59. M. Camberis, G. Le Gros, J. Urban Jr., Animal model of *Nippostrongylus brasiliensis* and *Heligmosomoides polygyrus*, in *Current Protocols in Immunology* (Wiley, 2003), chap. 19.
60. M. D. Robinson, D. J. McCarthy, G. K. Smyth, edgeR: A Bioconductor package for differential expression analysis of digital gene expression data. *Bioinformatics* **26**, 139–140 (2010).
61. Y. Zhang, T. Liu, C. A. Meyer, J. Eeckhoute, D. S. Johnson, B. E. Bernstein, C. Nusbaum, R. M. Myers, M. Brown, W. Li, X. S. Liu, Model-based analysis of ChIP-Seq (MACS). *Genome Biol.* **9**, R137 (2008).
62. A. R. Quinlan, I. M. Hall, BEDTools: A flexible suite of utilities for comparing genomic features. *Bioinformatics* **26**, 841–842 (2010).
63. Y. Liao, G. K. Smyth, W. Shi, featureCounts: An efficient general purpose program for assigning sequence reads to genomic features. *Bioinformatics* **30**, 923–930 (2014).
64. W. J. Kent, A. S. Zweig, G. Barber, A. S. Hinrichs, D. Karolchik, BigWig and BigBed: Enabling browsing of large distributed datasets. *Bioinformatics* **26**, 2204–2207 (2010).
65. M. T. Weirauch, A. Yang, M. Albu, A. G. Cote, A. Montenegro-Montero, P. Drewe, H. S. Najafabadi, S. A. Lambert, I. Mann, K. Cook, H. Zheng, A. Goity, H. van Bakel, J.-C. Lozano, M. Galli, M. G. Lewsey, E. Huang, T. Mukherjee, X. Chen, J. S. Reece-Hoyes, S. Govindarajan, G. Shaulsky, A. J. M. Walhout, F.-Y. Bouget, G. Ratsch, L. F. Larrondo, J. R. Ecker, T. R. Hughes, Determination and inference of eukaryotic transcription factor sequence specificity. *Cell* **158**, 1431–1443 (2014).
66. M. Huang, J. Wang, E. Torre, H. Dueck, S. Shaffer, R. Bonasio, J. I. Murray, A. Raj, M. Li, N. R. Zhang, SAVER: Gene expression recovery for single-cell RNA sequencing. *Nat. Methods* **15**, 539–542 (2018).
67. Y. Hao, S. Hao, E. Andersen-Nissen, W. M. Mauck III, S. Zheng, A. Butler, M. J. Lee, A. J. Wilk, C. Darby, M. Zager, P. Hoffman, M. Stoeckius, E. Papalexi, E. P. Mimitou, J. Jain, A. Srivastava, T. Stuart, L. M. Fleming, B. Yeung, A. J. Rogers, J. M. McElrath, C. A. Blish, R. Gottardo, P. Smibert, R. Satija, Integrated analysis of multimodal single-cell data. *Cell* **184**, 3573–3587.e29 (2021).
68. J. M. Granja, M. R. Corces, S. E. Pierce, S. T. Bagdatli, H. Choudhry, H. Y. Chang, W. J. Greenleaf, ArchR is a scalable software package for integrative single-cell chromatin accessibility analysis. *Nat. Genet.* **53**, 403–411 (2021).
69. D. Machlab, L. Burger, C. Soneson, F. M. Rijli, D. Schübeler, M. B. Stadler, monaLisa: An R/Bioconductor package for identifying regulatory motifs. *Bioinformatics* **38**, 2624–2625 (2022).
70. L. A. Pobezinsky, R. Etzensperger, S. Jeurling, A. Alag, T. Kadakia, T. M. McCaughtry, M. Y. Kimura, S. O. Sharrow, T. I. Guinter, L. Feigenbaum, A. Singer, Let-7 microRNAs target the lineage-specific transcription factor PLZF to regulate terminal NKT cell differentiation and effector function. *Nat. Immunol.* **16**, 517–524 (2015).
71. C. Trapnell, L. Pachter, S. L. Salzberg, TopHat: Discovering splice junctions with RNA-Seq. *Bioinformatics* **25**, 1105–1111 (2009).
72. R. J. Kinsella, A. Kahari, S. Haider, J. Zamora, G. Proctor, G. Spudich, J. Almeida-King, D. Staines, P. Derwent, A. Kerhornou, P. Kersey, P. Flicek, Ensembl BioMarts: A hub for data retrieval across taxonomic space. *Database* **2011**, bar030 (2011).
73. J. D. Buenrostro, B. Wu, H. Y. Chang, W. J. Greenleaf, ATAC-seq: A method for assaying chromatin accessibility genome-wide. *Curr. Protoc. Mol. Biol.* **109**, 10.1002/0471142727.mb2129s109 (2015).
74. M. R. Corces, A. E. Trevino, E. G. Hamilton, P. G. Greenside, N. A. Sinnott-Armstrong, S. Vesuna, A. T. Satpathy, A. J. Rubin, K. S. Montine, B. Wu, A. Kathiria, S. W. Cho, M. R. Mumbach, A. C. Carter, M. Kasowski, L. A. Orloff, V. I. Risca, A. Kundaje, P. A. Khavari, T. J. Montine, W. J. Greenleaf, H. Y. Chang, An improved ATAC-seq protocol reduces background and enables interrogation of frozen tissues. *Nat. Methods* **14**, 959–962 (2017).
75. B. Langmead, S. L. Salzberg, Fast gapped-read alignment with Bowtie 2. *Nat. Methods* **9**, 357–359 (2012).
76. H. Li, B. Handsaker, A. Wysoker, T. Fennell, J. Ruan, N. Homer, G. Marth, G. Abecasis, R. Durbin, The Sequence Alignment/Map format and SAMtools. *Bioinformatics* **25**, 2078–2079 (2009).
77. H. Yoshida, C. A. Lareau, R. N. Ramirez, S. A. Rose, B. Maier, A. Wroblewska, F. Desland, A. Chudnovskiy, A. Mortha, C. Dominguez, J. Tellier, E. Kim, D. Dwyer, S. Shinton, T. Nabekura, Y. Qi, B. Yu, M. Robinette, K.-W. Kim, A. Wagers, A. Rhoads, S. L. Nutt, B. D. Brown, S. Mostafavi, J. D. Buenrostro, C. Benoist, The cis-regulatory atlas of the mouse immune dystem. *Cell* **176**, 897–912.e20 (2019).
78. F. Ramírez, D. P. Ryan, B. Grüning, V. Bhardwaj, F. Kilpert, A. S. Richter, S. Heyne, F. Dündar, T. Manke, deepTools2: A next generation web server for deep-sequencing data analysis. *Nucleic Acids Res.* **44**, W160–W165 (2016).

79. U. Raudvere, L. Kolberg, I. Kuzmin, T. Arak, P. Adler, H. Peterson, J. Vilo, g:Profiler: A web server for functional enrichment analysis and conversions of gene lists (2019 update). *Nucleic Acids Res*. **47**, W191–W198 (2019).
80. A. N. Schep, B. Wu, J. D. Buenrostro, W. J. Greenleaf, chromVAR: Inferring transcription-factor-associated accessibility from single-cell epigenomic data. *Nat. Methods* **14**, 975–978 (2017).

Acknowledgments: We thank the Cornell Center for Animal Resource and Education (CARE) for expert mouse breeding assistance. Cell sorting was done at Cornell University's Flow Cytometry Facility (RRID:SCR_021740) in the Biotechnology Resource Center (BRC). Bulk RNA-seq and ATAC-seq profiling projects were coordinated and performed by the Transcriptional Regulation and Expression Facility (RRID:SCR_022532); single-cell 10x Genomics libraries were prepared, and all Illumina sequencing was conducted at the BRC Genomics Facility (RRID:SCR_021727) at Cornell University. We thank E. Fogarty for assistance with single-cell genomic assays. Lung homogenate RNA extraction and Influenza A virus qPCR were performed at the Animal Health Diagnostic Center (AHDC) at Cornell University. Human cells were collected and processed at the Golisano Children's Hospital, University of Rochester Medical Center, as part of the Respiratory Pathogens Research Center (NIAID HHSN272201200005C). **Funding:** This work was supported by National Institute of Health awards R01AI105265 (to B.D.R, from the National Institute of Allergy and Infectious Disease), R01AI110613, U01AI131348 (to B.D.R and A.G., from the National Institute of Allergy and Infectious Disease), P50HD076210 (to A.G., from National Institute of Child Health and Human Development), R01AI130379 (to E.D.T.W., from the National Institute of Allergy and Infectious Disease), and R21AI138025 (to N.L.S., from the National Institute of Allergy and Infectious Disease). M.P.D. is supported by an NHMRC (Australia) Senior Research Fellowship (1173027). K.M.S. was supported by K08AI108870. **Author contributions:** N.B.W., R.K.P., and C.K. planned and performed experiments, analyzed and interpreted data, and wrote the manuscript. O.O.O., C.T., J.W., S.P.W., K.J.Y.M., A.J.M., S.A.P., and K.N. performed experiments. N.L. and M.P.D. analyzed and interpreted the data. N.L.S., J.K.G., J.V., K.M.S. and E.D.T.W. planned experiments, analyzed, and interpreted data. A.G. and B.D.R. conceptualized the study, planned experiments, analyzed and interpreted data, and wrote the manuscript. **Competing interests:** The authors declare that they have no competing interests. **Data and materials availability:** The accession number for the RNA-seq, ATAC-seq, scRNA-seq, and scATAC-seq data reported here is GEO SuperSeries: GSE180732. RNA-seq samples GSM5469159, GSM5469160, and GSM5469161 were not used for the present study but instead correspond to our related bioRxiv submission. Tabulated data underlying the figures are included in data file S13. All other data needed to support the conclusions of the paper are present in the paper or the Supplementary Materials.

Submitted 18 November 2022
Resubmitted 28 August 2023
Accepted 26 January 2024
Published 23 February 2024
10.1126/sciimmunol.adf8776